Discrete-fracture-model of multi–scale time-splitting two–phase flow including nanoparticles transport in fractured porous media

Accepted Manuscript

Discrete-fracture-model of multi–scale time-splitting two–phase flow including nanoparticles transport in fractured porous media

Mohamed F. El-Amin, Jisheng Kou, Shuyu Sun

PII: S0377-0427(17)30568-X
DOI: https://doi.org/10.1016/j.cam.2017.11.008
Reference: CAM 11380

To appear in: *Journal of Computational and Applied Mathematics*

Received date : 8 December 2016
Revised date : 2 October 2017

Please cite this article as: M.F. El-Amin, J. Kou, S. Sun, Discrete-fracture-model of multi–scale time-splitting two–phase flow including nanoparticles transport in fractured porous media, *Journal of Computational and Applied Mathematics* (2017), https://doi.org/10.1016/j.cam.2017.11.008

Discrete-Fracture-Model of Multi–Scale Time-Splitting Two–phase Flow Including Nanoparticles Transport in Fractured Porous Media

Mohamed F El-Amin[a,b,c], Jisheng Kou[d], Shuyu Sun[c]

[a] *College of Engineering, Effat University, Jeddah 21478, Kingdom of Saudi Arabia.*
[b] *Mathematics Department, Faculty of Science, Aswan University, Aswan 81528, Egypt.*
[c] *Computational Transport Phenomena Laboratory (CTPL), Division of Physical Sciences and Engineering (PSE), King Abdullah University of Science and Technology (KAUST), Thuwal, Kingdom of Saudi Arabia.*
[d] *School of Mathematics and Statistics, Hubei Engineering University, Xiaogan 432000, Hubei, China.*

Abstract

In this article, we consider a two-phase immiscible incompressible flow including nanoparticles transport in fractured heterogeneous porous media. The system of the governing equations consists of water saturation, Darcy's law, nanoparticles concentration in water, deposited nanoparticles concentration on the pore-wall, and entrapped nanoparticles concentration in the pore-throat, as well as, porosity and permeability variation due to the nanoparticles deposition/entrapment on/in the pores. The discrete-fracture model (DFM) is used to describe the flow and transport in fractured porous media. Moreover, multiscale time-splitting strategy has been employed to manage different time-step sizes for different physics, such as saturation, concentration, etc. Numerical examples are provided to demonstrate the efficiency of the proposed multi-scale time splitting approach.

Keywords: Multiscale time-splitting, IMPES, nanoparticles, two-phase flow, porous media, reservoir simulation

1. Introduction

The fractured porous media are mainly composed of two heterogeneous parts, namely, matrices and fractures. The fractures have higher permeability than the matrix, but contains very small volume of fluid (porosity) compare to the matrix. Therefore, different scales are encountered in fractured porous media, and usually, dual-continua and discrete-fracture models are employed in modeling [1]–[14]. Warren and Root [14] have developed an idealized model to study the behavior flow in fractured porous media based on dual continua models. Dual–Porosity model was used when two porosity values existed in the domain. The dual–continua models (such as dual–porosity/dual–permeability model) [2], [6]–[8], [11], [12], [14] treat the matrix blocks and the fractures as two separate continua, that are theoretically interconnected by fluid mass transfer across their interfaces. In the discrete–fracture–model (DFM)[2], [9], [10], the fracture is treated as a lower dimensional domain to reduce the contrast of geometric scales.

Nowadays, nanoparticles injection into oil reservoirs is considered as an enhanced oil recovery method. Ju et al. [33] introduced a two-phase model with nanoparticles transport in porous media based on the modeling of particle migration through porous media [34]. El-Amin et al. [35, 36, 37] developed the model of transport in a two-phase flow in porous media, then, they

introduced numerical and dimensional analysis for the problem [38]. Salama et al. [39] studied the problem of nanoparticles transport in anisotropic porous media using the multipoint flux approximation. Recently, Chen et al. [40] presented a numerical simulation of drag reduction effects by hydrophobic nanoparticles adsorption method in water flooding processes. Chen et al. [41] have considered the dynamic update of anisotropic permeability field during the transport of nanoparticles in the subsurface.

In order to solve the system of equations that governing the two–phase flow in porous media, the IMplicit Pressure Explicit Saturation (IMPES) scheme can be used (e.g. [15, 16, 17, 18]). In IMPES scheme, the pressure equation is solved implicitly while the saturation is treated explicitly. The IMPES is a conditionally stable approach, hence it takes very small time step size, in particular with heterogeneous porous media. On the other hand, the temporal discretization has a significant effect on the efficiency of numerical simulators. Hence, employing traditional single-scale temporal scheme is restricted by the rapid of changes of the pressure and saturation with capillarity and concentrations in matrix or fracture if applicable. Therefore, the multiscale time splitting strategy is considered one of a significant improvement to treating the gap between the pressure and the saturation. Multiscale time splitting method has been considered in a number of publications such as, [20]–[29]. Similar methodology has been used to the problem of flow and transport simulations in fractured porous media [24]. VanderKwaak [30] used a hybrid implicit-explicit scheme by treating implicitly some portions

of the domain under certain stability conditions, while the rest of the domain is treated by the explicit time-stepping approach. Kou et al. [19] have developed a multiscale time–splitting strategy for simulating two–phase flow in fractured porous media. In [42] we have introduced nonlinear iterative IMPES-IMC (IMplicit Pressure Explicit Saturation–IMplicit Concentration) scheme to solve the flow equation of the model of nanoparticles transport in porous media. Recently, El-Amin et al. [43] presented a convergence analysis of the nonlinear iterative IMPES-IMC method for a two-phase flow in porous media associated with nanoparticle injection.

In the current article, we present a multiscale time-stepping technique for the modeling and simulation of nanoparticles transport with a two-phase flow in fractured porous media. An IMPES-IMC scheme is employed for the numerical treatment and the capillary pressure is treated implicitly, while the CCFD technique is used for the spatial discretization. We use a large time-step size in the matrix domain,while we use a smaller one in the fractures. Also, the time-step of the fractures pressure is partitioned to subtime-steps, then, we update the saturation in the same level of time-discretization explicitly. On the other hand, the saturation employs a coarse time-stepping in the matrix blocks, while a fine time-stepping in the fractures. We employ a similar time-splitting strategy of saturation for concentration equations. Finally, several numerical examples are provided to show the efficiency of the proposed scheme. The paper is organized as follows: The second section is devoted to the modeling and mathematical formulation. The third sec-

tion is devoted to the multiscale time-stepping technique with CCFD spatial discretization including subsections about time-splitting techniques in matrix and fracture for different physics such as pressure, saturation, and concentration. Then, Sec. 4 is devoted to numerical tests, and finally, the conclusions are drawn in Sec. 5.

2. Modeling and Mathematical Formulation

2.1. Governing equations

This paper considers the problem of nanoparticles transport with a two-phase immiscible incompressible flow in porous media, the system of governing equations consists of water saturation, Darcy's law, nanoparticles concentration, deposited nanoparticles concentration on the pore-wall, and entrapped nanoparticles concentration in the pore-throat. Also, the porosity and permeability vary due to the nanoparticles deposition/entrapment on/in the pores. In the following we introduce the governing equations briefly, (for details see Refs. [35, 36, 37, 38, 39, 41, 42]):

2.1.1. Momentum Conservation (Darcy's Law):

$$\mathbf{u}_\alpha = -\frac{k_\alpha}{\mu_\alpha}\nabla P_\alpha, \qquad \alpha = w, n, \tag{1}$$

where $\mathbf{K}$ is the permeability tensor $\mathbf{K} = k\mathbf{I}$, $\mathbf{I}$ is the identity matrix and k is a positive real number. ϕ is the porosity. $\mathbf{u}_\alpha, P_\alpha, \mu_\alpha, k_{r\alpha}$ are, respectively,

the velocity, the pressure, the viscosity and the relative permeability of the phase α.

2.1.2. Mass Conservation (Saturation Equation):

$$\phi \frac{\partial S_\alpha}{\partial t} + \nabla \cdot \mathbf{u}_\alpha = q_\alpha, \quad \alpha = w, n, \tag{2}$$

$$S_w + S_n = 1.$$

where S_α is the saturation of the phase α and q_α is the external mass flow rate.

2.1.3. Flow Equations Reformulation:

Providing the following definitions:

The capillary pressure: $P_c(S_w) = P_n - P_w$.

The total velocity: $\mathbf{u}_t = \mathbf{u}_w + \mathbf{u}_n$.

The flow fraction: $f_w = \lambda_w / \lambda_t$.

The phase mobility: $\lambda_\alpha = k_{r\alpha}/\mu_\alpha$.

The total mobility: λ_t.

The total source mass transfer: $q_t = q_w + q_n$.

After some mathematical manipulations and referring to Refs. [31], the pressure equation can be rewritten as,

$$\nabla \cdot \mathbf{u}_t = -\nabla \cdot \lambda_t \mathbf{K} \nabla P_w - \nabla \cdot \lambda_n \mathbf{K} \nabla P_c = q_t. \tag{3}$$

Because this equation contents the capillary pressure which is a function of saturation, it will be coupled with the following saturation equation to calculate the pressure:

$$\phi \frac{\partial S_w}{\partial t} - q_w = \nabla \cdot \lambda_w \mathbf{K} \nabla P_w. \tag{4}$$

However, the saturation is updated using the following form,

$$\phi \frac{\partial S_w}{\partial t} - q_w = -\nabla \cdot (f_w \mathbf{u}_a). \tag{5}$$

where $\mathbf{u}_w = f_w \mathbf{u}_a$ and $\mathbf{u}_a = -\lambda_t \mathbf{K} \nabla P_w$.

2.1.4. Nanoparticles Transport:

Assuming that the nanoparticles exists only in the water phase of one size interval. So, the transport equation of the nanoparticles in the water phase is given as ([32, 33, 34, 35, 36, 37, 38, 39, 41, 42]),

$$\phi \frac{\partial (S_w C)}{\partial t} + \nabla \cdot (\mathbf{u}_w C - \phi S_w D \nabla C) = R + Q_c, \tag{6}$$

where C is the nanoparticles concentrations. D is the Brownian diffusion. Q_c is the rate of change of particle volume belonging to a source/sink term. R is the net rate of loss of nanoparticles which is defined by,

$$R = \frac{\partial C_{s1}}{\partial t} + \frac{\partial C_{s2}}{\partial t} \tag{7}$$

2.1.5. Nanoparticles Surface Deposition:

The surface deposition is expressed by,

$$\frac{\partial C_{s1}}{\partial t} = \begin{cases} \gamma_d |\mathbf{u}_w| C, & \mathbf{u}_w \leq u_r \\ \\ \gamma_d |\mathbf{u}_w| C - \gamma_e |\mathbf{u}_w - u_r| C_{s1}, & \mathbf{u}_w > u_r \end{cases} \tag{8}$$

where C_{s1} is the deposited nanoparticles concentration on the pore surfaces of the porous medium. γ_d is the rate coefficients for surface retention of the nanoparticles. γ_e is the rate coefficients for entrainment of the nanoparticles. u_r is the critical velocity of the water phase.

2.1.6. Nanoparticles Throat Entrapment:

The rate of entrapment of the nanoparticles is,

$$\frac{\partial C_{s2}}{\partial t} = \gamma_{pt} |\mathbf{u}_w| C, \tag{9}$$

where C_{s2} is the entrapped nanoparticles concentration in pore throats and γ_{pt} is the pore throat blocking constants.

2.2. Porosity and Permeability Variations

If a particle is larger than a pore throat may block at the pore throat (for example in the case of nanopore) during nanoparticles transport. It may cause blocking of the porous medium, or in general, it could cause changing in porosity and permeability due to nanoparticles precipitation on the walls and

throats of the pores. So, solid properties such as porosity and permeability may be slightly changed due to nanoparticles precipitation on the walls and throats of the pores. Therefore, it may be neglected in the regular cases but in general, it is worth to investigate. The porosity variation may be defined as,

$$\phi = \phi_0 - \delta\phi \tag{10}$$

where ϕ_0 is the initial porosity and,

$$\delta\phi = C_{s1} + C_{s2}, \tag{11}$$

is the porosity change due to release or retention of nanoparticles. On the other hand, the change in permeability due to nanoparticles deposition on the pore–walls and entrapped in the pore–throats is represented as [33],

$$\mathbf{K} = \mathbf{K}_0 \left[(1-f)\, k_f + f \frac{\phi}{\phi_0} \right]^l, \tag{12}$$

$$f = 1 - \gamma_f C_{s2} \tag{13}$$

where $\mathbf{K}_0$ is the initial permeability, k_f is constant for fluid seepage, γ_f is the coefficient of flow efficiency for the particles and $2.5 \leq l \leq 3.5$ is constant. For the nanoparticles transport carried by the fluid stream in the porous media, deposition on pore surfaces and blockage in pore throats may occur. The retained particles on pore surfaces may desorb for hydrodynamic forces, and then possibly adsorb on other sites of the pore bodies or get entrapped

at other pore throats.

2.3. Initial and Boundary Conditions:

Consider the computational domain Ω with the boundary $\partial\Omega$ which is subjected to Dirichlet Γ_D and Neumann Γ_N boundaries, where $\partial\Omega = \Gamma_D \cup \Gamma_N$ and $\Gamma_D \cap \Gamma_N = \emptyset$. At the beginning of the injection process, we have,

$$S_w = S_w^0, \quad C = C_{s1} = C_{s2} = 0 \quad \text{in} \quad \Omega \qquad \text{at} \quad t = 0, \tag{14}$$

The boundary conditions are given as,

$$P_w \,(\text{or } P_n) = P^D \quad \text{on} \quad \Gamma_D, \tag{15}$$

$$\mathbf{u}_t \cdot \mathbf{n} = q^N, \quad S_w = S^N, \quad C = C_0, \quad C_{s1} = C_{s2} = 0 \quad \text{on} \quad \Gamma_N. \tag{16}$$

where $\mathbf{n}$ is the outward unit normal vector to $\partial\Omega$, P^D is the pressure on Γ_D and q^N the imposed inflow rate on Γ_N, respectively.

2.4. Discrete-Fracture Model

In order to represent the fractures explicitly in the fractured porous media, we use the discrete-fracture model (DFM) [5, 45]. In the DFM, the fracture gridcells are simplified as the matrix gridcell interfaces and the fractures are surrounded by the matrix blocks. Thus, if the matrix gridcells are of n-dimension, then, the fracture gridcells are of $(n-1)$-dimension. The domain is decomposed into the matrix domain, Ω_{m} and fracture domain, Ω_{f}.

The pressure equation in the matrix domain is given by,

$$-\nabla \cdot \lambda_{t,\mathrm{m}} \mathbf{K}_{\mathrm{m}} \nabla P_{w,\mathrm{m}} - \nabla \cdot \lambda_{n,\mathrm{m}} \mathbf{K}_{\mathrm{m}} \nabla P_{c,\mathrm{m}} = q_{t,\mathrm{m}}, \tag{17}$$

Assuming that the pressure and saturation along the fracture width are constants, and by integration, the pressure equation in the fracture becomes,

$$-\nabla \cdot \lambda_{t,\mathrm{f}} \mathbf{K}_{\mathrm{f}} \nabla P_{w,\mathrm{f}} - \nabla \cdot \lambda_{n,\mathrm{f}} \mathbf{K}_{\mathrm{f}} \nabla P_{c,\mathrm{f}} = q_{t,\mathrm{f}} + Q_{t,\mathrm{f}}, \tag{18}$$

The matrix-fracture interface condition is given by,

$$P_{w,\mathrm{m}} = P_{w,\mathrm{f}}, \quad P_{c,\mathrm{m}} = P_{c,\mathrm{f}}, \quad \text{on} \;\; \partial\Omega_{\mathrm{m}} \cap \Omega_{\mathrm{f}}. \tag{19}$$

where the subscript m represents the matrix domain, while the subscript f represents the fracture domain. $Q_{t,\mathrm{f}}$ is the mass transfer across the matrix-fracture interfaces.

Similarly, the saturation equation in the matrix domain can be written as,

$$\phi_{\mathrm{m}} \frac{\partial S_{w,\mathrm{m}}}{\partial t} - \nabla \cdot \lambda_{w,\mathrm{m}} \mathbf{K}_{\mathrm{m}} \nabla P_{w,\mathrm{m}} = q_{w,\mathrm{m}}, \tag{20}$$

On the other hand, the saturation equation, will be used to rebuild the coupling relationship between the pressure and saturation, in the fracture system is given by,

$$\phi_{\mathrm{f}} \frac{\partial S_{w,\mathrm{f}}}{\partial t} - \nabla \cdot \lambda_{w,\mathrm{f}} \mathbf{K}_{\mathrm{f}} \nabla P_{w,\mathrm{f}} = q_{w,\mathrm{f}} + Q_{w,\mathrm{f}}, \tag{21}$$

where $Q_{w,\mathrm{f}}$ represents the mass transfer across the matrix-fracture interfaces,

$$Q_{w,\mathrm{f}} = (\lambda_{w,\mathrm{f}}\mathbf{K}_{\mathrm{f}}\nabla P_{w,\mathrm{f}}) \cdot \mathbf{n}.$$

where $\mathbf{n}$ is a normal unit vector from matrix to fracture. The second form of the saturation equation which is used to update the saturation, is expressed in the matrix domain as,

$$\phi_{\mathrm{m}}\frac{\partial S_{w,\mathrm{m}}}{\partial t} + \nabla \cdot (f_{w,\mathrm{m}}\mathbf{u}_{a,\mathrm{m}}) = q_{w,\mathrm{m}}, \tag{22}$$

and in the fracture domain it is given as,

$$\phi_{\mathrm{f}}\frac{\partial S_{w,\mathrm{f}}}{\partial t} + \nabla \cdot (f_{w,\mathrm{f}}\mathbf{u}_{a,\mathrm{f}}) = q_{w,\mathrm{f}} + \widehat{Q}_{w,\mathrm{f}}, \tag{23}$$

where $\widehat{Q}_{w,\mathrm{f}}$ is given as,

$$\widehat{Q}_{w,\mathrm{f}} = (f_{w,\mathrm{f}}\mathbf{u}_{a,\mathrm{f}}) \cdot \mathbf{n}.$$

where $\mathbf{n}$ is a normal unit vector from matrix to fracture. The nanoparticles transport equation in the matrix domain may be expressed as,

$$\phi_{\mathrm{m}}\frac{\partial (S_{w,\mathrm{m}}C_{\mathrm{m}})}{\partial t} + \nabla \cdot (\mathbf{u}_{w,\mathrm{m}}C_{\mathrm{m}} - \phi_{\mathrm{m}}S_{w,\mathrm{m}}D\nabla C_{\mathrm{m}}) = R_{\mathrm{m}} + Q_{c,\mathrm{m}}, \tag{24}$$

where C_{m} is the nanoparticles concentrations in the matrix domain. $Q_{c,\mathrm{m}}$ is the rate of change of particle volume belonging to a source/sink term in the matrix domain. R_{m} is the net rate of loss of nanoparticles in the matrix

domain. On the other hand, the nanoparticles transport equation in the fracture domain is given by,

$$\phi_{\mathrm{f}}\frac{\partial\left(S_{w,\mathrm{f}}C_{\mathrm{f}}\right)}{\partial t}+\nabla\cdot\left(\mathbf{u}_{w,\mathrm{f}}C_{\mathrm{f}}-\phi_{\mathrm{f}}S_{w,\mathrm{f}}D\nabla C_{\mathrm{f}}\right)=R_{\mathrm{f}}+Q_{c,\mathrm{f}}+Q_{c,w,\mathrm{f}}, \tag{25}$$

where C_{f} is the nanoparticles concentrations in the fracture domain. $Q_{c,\mathrm{f}}$ is the rate of change of particle volume belonging to a source/sink term in the fracture domain. R_{f} is the net rate of loss of nanoparticles in the fracture domain. $Q_{c,w,\mathrm{f}}$ represents the rate of change of particle volume across the matrix-fracture interfaces,

$$Q_{c,w,\mathrm{f}}=\left(\mathbf{u}_{w,\mathrm{f}}C_{\mathrm{f}}-\phi_{\mathrm{f}}S_{w,\mathrm{f}}D\nabla C_{\mathrm{f}}\right)\cdot\mathbf{n}.$$

where $\mathbf{n}$ is a normal unit vector from matrix to fracture. The interface condition of the nanoparticles concentration is,

$$C_{\mathrm{m}}=C_{\mathrm{f}},\quad \text{on}\quad \partial\Omega_{\mathrm{m}}\cap\Omega_{\mathrm{f}}. \tag{26}$$

The surface deposition in the matrix domain is given by,

$$\frac{\partial C_{s1,\mathrm{m}}}{\partial t}=\begin{cases}\gamma_d|\mathbf{u}_{w,\mathrm{m}}|C_{\mathrm{m}}, & \mathbf{u}_{w,\mathrm{m}}\leq u_r\\ \gamma_d|\mathbf{u}_{w,\mathrm{m}}|C_{\mathrm{m}}-\gamma_e|\mathbf{u}_{w,\mathrm{m}}-u_r|C_{s1,\mathrm{m}}, & \mathbf{u}_{w,\mathrm{m}}>u_r\end{cases} \tag{27}$$

where $C_{s1,\mathrm{m}}$ is the deposited nanoparticles concentration on the pore surfaces

of the matrix domain. Similarly, surface deposition in the fracture domain is represented by,

$$\frac{\partial C_{s1,\mathrm{f}}}{\partial t} = \begin{cases} \gamma_d |\mathbf{u}_{w,\mathrm{f}}| C_{\mathrm{f}}, & \mathbf{u}_{w,\mathrm{f}} \leq u_r \\ \\ \gamma_d |\mathbf{u}_{w,\mathrm{f}}| C_{\mathrm{f}} - \gamma_e |\mathbf{u}_{w,\mathrm{f}} - u_r| C_{s1,\mathrm{f}}, & \mathbf{u}_{w,\mathrm{f}} > u_r \end{cases} \tag{28}$$

where $C_{s1,\mathrm{f}}$ is the deposited nanoparticles concentration on the pore surfaces of the fracture domain with the interface condition,

$$C_{s1,\mathrm{m}} = C_{s1,\mathrm{f}}, \quad \text{on} \quad \partial\Omega_{\mathrm{m}} \cap \Omega_{\mathrm{f}}. \tag{29}$$

Finally, the rate of entrapment of the nanoparticles in the matrix domain is written as,

$$\frac{\partial C_{s2,\mathrm{m}}}{\partial t} = \gamma_{pt} |\mathbf{u}_{w,\mathrm{m}}| C_{\mathrm{m}}, \tag{30}$$

where $C_{s2,\mathrm{m}}$ is the entrapped nanoparticles concentration in pore throats of matrix domain. Also, the rate of entrapment of the nanoparticles in the fractures is,

$$\frac{\partial C_{s2,\mathrm{f}}}{\partial t} = \gamma_{pt} |\mathbf{u}_{w,\mathrm{f}}| C_{\mathrm{f}} + Q_{Cs1,,\mathrm{m,f}}, \tag{31}$$

where $C_{s2,\mathrm{f}}$ is the entrapped nanoparticles concentration in pore throats of fracture with the following interface condition,

$$C_{s2,\mathrm{m}} = C_{s2,\mathrm{f}}, \quad \text{on} \quad \partial\Omega_{\mathrm{m}} \cap \Omega_{\mathrm{f}}. \tag{32}$$

3. Multi-Scale Time-Splitting and Spatial Discretization

In the multiscale time splitting method, we employ a different time step size for each time derivative term as they have different physics. For example, the time-step size for the pressure can be taken larger than those of saturation and nanoparticle concentrations. Also, the pressure in the fractures varies more rapidly than the matrix domain, we use a smaller time step size for the pressure in the fractures, and so on. For the spatial discretization, we use the cell-centered finite difference (CCFD) method, which is locally conservative and equivalent to the quadratic finite element method (see Ref. [44]). In general, the current scheme can be used with other spatial discretization schemes.

It is worthy to point out that the elliptic/parabolic components of the equation system (i.e. the pressure equations here) should be treated implicitly because otherwise the explicit-stepping CFL condition usually requires the time size less than $\mathrm{O}(h^2)$, with h being the spatial mesh size, which is too restrictive for our applications. The treatment of the hyperbolic component of the equation system (i.e. the saturation equation), however, can be implicit or explicit, or even semi-implicit. The explicit-stepping CFL condition for hyperbolic equation requires the time step to be $C_t h$ only, providing possibility of explicit treatment. For convenience, in this paper we consider explicit treatment of the saturation equation in both fractures and matrix. We note that, there were works in the literature [48, 49] to use explicit time-stepping for the saturation equation in matrix, but implicit treatment in

fractures. This is because the CFL requirement of $C_t h$ has quite dramatic difference constant C_t in fractures and in matrix, with usually much smaller C_t in fractures as compared to it in matrix. Thus, one might want to use implicit treatment in fractures to avoid the otherwise very restrictive time step condition.

3.1. Multi-Scale Time-Splitting Approach for pressure

Now, let us introduce the time discretization for the pressure in the matrix domain. We divide the total time interval $[0, T]$ into $N_{p,\mathrm{m}}$ steps, i.e., $0 = t^0 < t^1 < \cdots < t^{N_{p,\mathrm{m}}} = T$ and the time step length is $\triangle t^i = t^{i+1} - t^i$. We use a smaller time step size for the pressure in the fractures because the pressure in the fractures varies more rapidly than the pressure in the matrix domain. Thus, we divide each subinterval $(t^i, t^{i+1}]$ into $N_{p,\mathrm{f}}$ sub-subintervals as $(t^i, t^{i+1}] = \bigcup_{j=0}^{N_{p,\mathrm{f}}-1}(t^{i,j}, t^{i,j+1}]$, where $t^{i,0} = t^i$ and $t^{i,N_{p,\mathrm{f}}} = t^{i+1}$ and $\triangle t^{i,j} = t^{i,j+1} - t^{i,j}$.

Because the classical IMPES method is usually unstable, so, we employ an implicit approach to treating capillary pressure [18]. In the following, b refers to the boundary of the matrix gridcells K such that its area is $|K|$. The flux across the boundary b of the gridcell K is denoted by $\boldsymbol{\xi}$. On each interface $b \in \partial K \cap \partial K'$, $\mathbf{n}_b$ is the unit normal vector pointing from K to K'. $|b|$ is the length of b and $d_{K,K'}$ stands for the Euclidean distance between the central points of the cells K and K'. $d_{K,b}$ stands for the Euclidean distance from the central points of the cell K and the cell boundary b. For the case b

locating on the entire domain boundary, the pressure is provided by Dirichlet boundary conditions if $b \in \Gamma^D$, otherwise, the fluxes are determined by the Neumann conditions if $b \in \partial\Omega^N$.

The pressure equation in the matrix domain and fractures is written, respectively as,

$$-\nabla\cdot\lambda_t(S^i_{w,\mathrm{m}})\mathbf{K}_\mathrm{m}\nabla P^{i+1}_{w,\mathrm{m}}-\nabla\cdot\lambda_n(S^i_{w,\mathrm{m}})\mathbf{K}_\mathrm{m}\nabla((1-\omega)P^i_{c,\mathrm{m}}+\omega P^{i+1}_{c,\mathrm{m}}) = q^{i+1}_{t,\mathrm{m}}, \quad (33)$$

and

$$-\nabla\cdot\lambda_t(S^i_{w,\mathrm{f}})\mathbf{K}_\mathrm{f}\nabla P^{i+1}_{w,\mathrm{f}} - \nabla\cdot\lambda_n(S^i_{w,\mathrm{f}})\mathbf{K}_\mathrm{f}\nabla((1-\omega)P^i_{c,\mathrm{f}} + \omega P^{i+1}_{c,\mathrm{f}}) = q^{i+1}_{t,\mathrm{f}} + Q^{i+1}_{t,\mathrm{f}}. \quad (34)$$

where ω is the temporal discretization parameter. It is clear that the above equation, (33), is reduced to the classical IMPES scheme if $\omega = 0$. In (33) and (34), λ_w, λ_n and λ_t in the pressure equations are treated explicitly. Now, applying the CCFD scheme on (33), one obtains,

$$\sum_{b\in\partial K}\boldsymbol{\xi}^{i+1}_{a,\mathrm{m},b} + \sum_{b\in\partial K}((1-\omega)\boldsymbol{\xi}^i_{c,\mathrm{m},b} + \omega\boldsymbol{\xi}^{i+1}_{c,\mathrm{m},b}) = q^{i+1}_{t,\mathrm{m},K}|K|, \quad (35)$$

If $b \in \partial K \cap \partial K'$ and $b \nsubseteq \Omega_\mathrm{f}$, the fluxes in (35) are given by,

$$\boldsymbol{\xi}^{i+1}_{a,\mathrm{m},b} = -|b|\chi^i_{t,b}\frac{P^{i+1}_{w,\mathrm{m},K'} - P^{i+1}_{w,\mathrm{m},K}}{d_{K,K'}}, \quad (36)$$

$$\boldsymbol{\xi}^i_{c,\mathrm{m},b} = -|e|\chi^i_{n,b}\frac{P^i_{c,\mathrm{m},K'} - P^i_{c,\mathrm{m},K}}{d_{K,K'}}, \tag{37}$$

$$\boldsymbol{\xi}^{i+1}_{c,\mathrm{m},b} = -|b|\chi^i_{n,b}\frac{P^{i+1}_{c,\mathrm{m},K'} - P^{i+1}_{c,\mathrm{m},K}}{d_{K,K'}}, \tag{38}$$

where $\chi^i_{t,b}$ and $\chi^i_{n,b}$ are given by

$$\chi^i_{t,b} = \frac{d_{K,K'}\lambda^i_{t,\mathrm{m},K}\lambda^i_{t,\mathrm{m},K'}\mathbf{K}_{\mathrm{m},K}\mathbf{K}_{\mathrm{m},K'}}{d_{K,b}\lambda^i_{t,\mathrm{m},K'}\mathbf{K}_{\mathrm{m},K'} + d_{K',b}\lambda^i_{t,\mathrm{m},K}\mathbf{K}_{\mathrm{m},K}}, \tag{39}$$

$$\chi^i_{n,b} = \frac{d_{K,K'}\lambda^i_{n,\mathrm{m},K}\lambda^i_{n,\mathrm{m},K'}\mathbf{K}_{\mathrm{m},K}\mathbf{K}_{\mathrm{m},K'}}{d_{K,b}\lambda^i_{n,\mathrm{m},K'}\mathbf{K}_{\mathrm{m},K'} + d_{K',b}\lambda^i_{n,\mathrm{m},K}\mathbf{K}_{\mathrm{m},K}}. \tag{40}$$

On the other hand, if $b \in \Omega_{\mathrm{f}} \cap \partial K \cap \partial K'$ and b is a gridcell of the fracture system, we have

$$\boldsymbol{\xi}^{i+1}_{a,\mathrm{m},b} \equiv \boldsymbol{\xi}^{i+1}_{a,\mathrm{m},b,K} = -|b|\chi^i_{t,\mathrm{mf},b}\frac{P^{i+1}_{w,\mathrm{f},b} - P^{i+1}_{w,\mathrm{m},K}}{d_{K,b} + \frac{\epsilon}{2}}, \tag{41}$$

$$\boldsymbol{\xi}^{i}_{c,\mathrm{m},b} \equiv \boldsymbol{\xi}^{i}_{c,\mathrm{m},b,K} = -|b|\chi^i_{n,\mathrm{mf},b}\frac{P^{i}_{c,\mathrm{f},b} - P^{i}_{c,\mathrm{m},K}}{d_{K,b} + \frac{\epsilon}{2}}, \tag{42}$$

$$\boldsymbol{\xi}^{i+1}_{c,\mathrm{m},b} \equiv \boldsymbol{\xi}^{i+1}_{c,\mathrm{m},b,K} = -|b|\chi^i_{n,\mathrm{mf},b}\frac{P^{i+1}_{c,\mathrm{f},b} - P^{i+1}_{c,\mathrm{m},K}}{d_{K,b} + \frac{\epsilon}{2}}, \tag{43}$$

where $\chi^i_{t,\mathrm{mf},b}$ and $\chi^i_{n,\mathrm{mf},e}$ are given by

$$\chi^i_{t,\mathrm{mf},b} = \frac{(d_{K,b} + \frac{\epsilon}{2})\lambda^i_{t,\mathrm{f},K}\lambda^i_{t,\mathrm{m},K}\mathbf{K}_{\mathrm{f},K}\mathbf{K}_{\mathrm{m},K}}{\frac{\epsilon}{2}\lambda^i_{t,\mathrm{m},K}\mathbf{K}_{\mathrm{m},K} + d_{K,b}\lambda^i_{t,\mathrm{f},K}\mathbf{K}_{\mathrm{f},K}}, \tag{44}$$

$$\chi^i_{n,\mathrm{mf},b} = \frac{(d_{K,b} + \frac{\epsilon}{2})\lambda^i_{n,\mathrm{f},K}\lambda^i_{n,\mathrm{m},K}\mathbf{K}_{\mathrm{f},K}\mathbf{K}_{\mathrm{m},K}}{\frac{\epsilon}{2}\lambda^i_{n,\mathrm{m},K}\mathbf{K}_{\mathrm{m},K} + d_{K,b}\lambda^i_{n,\mathrm{f},K}\mathbf{K}_{\mathrm{f},K}}. \tag{45}$$

where ϵ is the fracture width. The above processes of deriving the equations (35)-(45) can also be carried out for the reduced-dimensional fracture system. Let b be a gridcell of the fracture network. The CCFD scheme is applied to (34), and then we have

$$\sum_{\gamma\in\partial b}\boldsymbol{\xi}^{i+1}_{a,\mathrm{f},\gamma}+\sum_{\gamma\in\partial b}((1-\omega)\boldsymbol{\xi}^{i}_{c,\mathrm{f},\gamma}+\omega\boldsymbol{\xi}^{i+1}_{c,\mathrm{f},\gamma})=q^{i+1}_{t,\mathrm{f},b}|b|+Q^{i+1}_{t,\mathrm{f},b}|b|, \tag{46}$$

where γ is the face of the gridcell b in the fracture network. $\boldsymbol{\xi}$ is the flux across the boundary γ of the fracture gridcell b. The matrix-fracture transfer is treated as a source term in the fracture system.

$$Q^{i+1}_{t,\mathrm{f},b}=-(Q^{i+1}_{t,\mathrm{f},b,K}+Q^{i+1}_{t,\mathrm{f},b,K'})/\epsilon, \tag{47}$$

$$Q^{i+1}_{t,\mathrm{f},b,K}=\boldsymbol{\xi}^{i+1}_{a,\mathrm{m},b,K}+(1-\omega)\boldsymbol{\xi}^{i}_{c,\mathrm{m},b,K}+\omega\boldsymbol{\xi}^{i+1}_{c,\mathrm{m},b,K}, \tag{48}$$

$$Q^{i+1}_{t,\mathrm{f},b,K'}=\boldsymbol{\xi}^{i+1}_{a,\mathrm{m},b,K'}+(1-\omega)\boldsymbol{\xi}^{i}_{c,\mathrm{m},b,K'}+\omega\boldsymbol{\xi}^{i+1}_{c,\mathrm{m},b,K'}, \tag{49}$$

where $\boldsymbol{\xi}^{i+1}_{a,\mathrm{m},b}, \boldsymbol{\xi}^{i}_{c,\mathrm{m},b}$ and $\boldsymbol{\xi}^{i+1}_{c,\mathrm{m},b}$ are defined in (41)-(43).

Now, let us consider the interface connecting multiple fractures. Let Λ_γ be the set composed of the fracture grid cells that are jointed by γ, the discretization of the mass conservation equation is,

$$\sum_{b\in\Lambda_\gamma}\left(\boldsymbol{\xi}^{i+1}_{a,\mathrm{f},\gamma,e}+(1-\omega)\boldsymbol{\xi}^{i}_{c,\mathrm{f},\gamma,b}+\omega\boldsymbol{\xi}^{i+1}_{c,\mathrm{f},\gamma,b}\right)=0, \tag{50}$$

where $\boldsymbol{\xi}_{a,\mathrm{f},\gamma,b}=\boldsymbol{\xi}_{a,\mathrm{f},\gamma}|_{\gamma\in b}$ and $\boldsymbol{\xi}_{c,\mathrm{f},\gamma,b}=\boldsymbol{\xi}_{c,\mathrm{f},\gamma}|_{\gamma\in b}$.

Combining the formulations in the matrix domain and fracture network, we obtain the discretization of total mass conservation equation given by

$$\begin{bmatrix} \mathbf{A}^i_{a,\mathrm{m},\mathrm{m}} & \mathbf{A}^i_{a,\mathrm{m},\mathrm{f}} \\ \mathbf{A}^i_{a,\mathrm{f},\mathrm{m}} & \mathbf{A}^i_{a,\mathrm{f},\mathrm{f}} \end{bmatrix} \begin{bmatrix} P^{i+1}_{w,\mathrm{m}} \\ P^{i+1}_{w,\mathrm{f}} \end{bmatrix} + \begin{bmatrix} \mathbf{A}^i_{c,\mathrm{m},\mathrm{m}} & \mathbf{A}^i_{c,\mathrm{m},\mathrm{f}} \\ \mathbf{A}^i_{c,\mathrm{f},\mathrm{m}} & \mathbf{A}^i_{c,\mathrm{f},\mathrm{f}} \end{bmatrix} \left\{ (1-\omega) \begin{bmatrix} P^i_{c,\mathrm{m}} \\ P^i_{c,\mathrm{f}} \end{bmatrix} + \omega \begin{bmatrix} P^{i+1}_{c,\mathrm{m}} \\ P^{i+1}_{c,\mathrm{f}} \end{bmatrix} \right\} = \begin{bmatrix} \mathbf{Q}^{i+1}_{ac,\mathrm{m}} \\ \mathbf{Q}^{i+1}_{ac,\mathrm{f}} \end{bmatrix}. \tag{51}$$

The capillary pressure $P_c(\mathbf{S}^{i+1}_w)$ is linearized w.r.t. $\mathbf{S}^i_w$ as,

$$P_c(\mathbf{S}^{i+1}_w) \simeq P_c(\mathbf{S}^i_w) + P'_c(\mathbf{S}^i_w)(\mathbf{S}^{i+1}_w - \mathbf{S}^i_w). \tag{52}$$

The backward Euler is used for time discretization as,

$$P_{\mathrm{m}} \frac{S^{i+1}_{w,\mathrm{m}} - S^i_{w,\mathrm{m}}}{\Delta t^i} - \nabla \cdot \lambda_w(S^i_{w,\mathrm{m}}) \mathbf{K}_{\mathrm{m}} \nabla P^{i+1}_{w,\mathrm{m}} = q^{i+1}_{w,\mathrm{m}}, \tag{53}$$

and

$$P_{\mathrm{f}} \frac{S^{i+1}_{w,\mathrm{f}} - S^i_{w,\mathrm{f}}}{\Delta t^i} - \nabla \cdot \lambda_w(S^i_{w,\mathrm{f}}) \mathbf{K}_{\mathrm{f}} \nabla P^{i+1}_{w,\mathrm{f}} = q^{i+1}_{w,\mathrm{f}} + Q^{i+1}_{w,\mathrm{f}}. \tag{54}$$

The CCFD discretization can be represented by,

$$\frac{1}{\Delta t^i}\begin{bmatrix} \mathbf{M}_{\mathrm{m}} & \\ & \mathbf{M}_{\mathrm{f}} \end{bmatrix}\begin{bmatrix} \mathbf{S}^{i+1}_{w,\mathrm{m}} - \mathbf{S}^{i}_{w,\mathrm{m}} \\ \mathbf{S}^{i+1}_{w,\mathrm{f}} - \mathbf{S}^{i}_{w,\mathrm{f}} \end{bmatrix} + \begin{bmatrix} \mathbf{A}^i_{w,\mathrm{m,m}} & \mathbf{A}^i_{w,\mathrm{m,f}} \\ \mathbf{A}^i_{w,\mathrm{f,m}} & \mathbf{A}^i_{w,\mathrm{f,f}} \end{bmatrix}\begin{bmatrix} P^{i+1}_{w,\mathrm{m}} \\ P^{i+1}_{w,\mathrm{f}} \end{bmatrix} = \begin{bmatrix} \mathbf{Q}^{i+1}_{w,\mathrm{m}} \\ \mathbf{Q}^{i+1}_{w,\mathrm{f}} \end{bmatrix}. \tag{55}$$

Substituting (52) and (55) into (51), we obtain the coupled pressure equation

$$\mathbf{A}^i_t \begin{bmatrix} P^{i+1}_{w,\mathrm{m}} \\ P^{i+1}_{w,\mathrm{f}} \end{bmatrix} = \mathbf{Q}^i_t, \tag{56}$$

where

$$\mathbf{A}^i_t = \begin{bmatrix} \mathbf{A}^i_{a,\mathrm{m,m}} & \mathbf{A}^i_{a,\mathrm{m,f}} \\ \mathbf{A}^i_{a,\mathrm{f,m}} & \mathbf{A}^i_{a,\mathrm{f,f}} \end{bmatrix} - \omega\Delta t^i \begin{bmatrix} \mathbf{A}^i_{c,\mathrm{m,m}} & \mathbf{A}^i_{c,\mathrm{m,f}} \\ \mathbf{A}^i_{c,\mathrm{f,m}} & \mathbf{A}^i_{c,\mathrm{f,f}} \end{bmatrix}\begin{bmatrix} P'_c(\mathbf{S}^i_{w,\mathrm{m}}) & \\ & P'_c(\mathbf{S}^i_{w,\mathrm{f}}) \end{bmatrix} \begin{bmatrix} \mathbf{M}^{-1}_{\mathrm{m}} & \\ & \mathbf{M}^{-1}_{\mathrm{f}} \end{bmatrix}\begin{bmatrix} \mathbf{A}^i_{w,\mathrm{m,m}} & \mathbf{A}^i_{w,\mathrm{m,f}} \\ \mathbf{A}^i_{w,\mathrm{f,m}} & \mathbf{A}^i_{w,\mathrm{f,f}} \end{bmatrix}, \tag{57}$$

and

$$\mathbf{Q}^i_t = \begin{bmatrix} \mathbf{Q}^{i+1}_{ac,\mathrm{m}} \\ \mathbf{Q}^{i+1}_{ac,\mathrm{f}} \end{bmatrix} - \begin{bmatrix} \mathbf{A}^i_{c,\mathrm{m,m}} & \mathbf{A}^i_{c,\mathrm{m,f}} \\ \mathbf{A}^i_{c,\mathrm{f,m}} & \mathbf{A}^i_{c,\mathrm{f,f}} \end{bmatrix}\begin{bmatrix} P_c(\mathbf{S}^i_{w,\mathrm{m}}) \\ P_c(\mathbf{S}^i_{w,\mathrm{f}}) \end{bmatrix} - \omega\Delta t^i \begin{bmatrix} \mathbf{A}^i_{c,\mathrm{m,m}} & \mathbf{A}^i_{c,\mathrm{m,f}} \\ \mathbf{A}^i_{c,\mathrm{f,m}} & \mathbf{A}^i_{c,\mathrm{f,f}} \end{bmatrix} \begin{bmatrix} P'_c(\mathbf{S}^i_{w,\mathrm{m}}) & \\ & P'_c(\mathbf{S}^i_{w,\mathrm{f}}) \end{bmatrix}\begin{bmatrix} \mathbf{M}^{-1}_{\mathrm{m}} & \\ & \mathbf{M}^{-1}_{\mathrm{f}} \end{bmatrix}\begin{bmatrix} \mathbf{Q}^{i+1}_{w,\mathrm{m}} \\ \mathbf{Q}^{i+1}_{w,\mathrm{f}} \end{bmatrix}. \tag{58}$$

The pressure equation in the fractures at each time subtime-step is given by,

$$-\nabla\cdot\lambda_t(S_{w,\mathrm{f}}^{i,j})\mathbf{K}_\mathrm{f}\nabla P_{w,\mathrm{f}}^{i,j+1}-\nabla\cdot\lambda_n(S_{w,\mathrm{f}}^{i,j})\mathbf{K}_\mathrm{f}\nabla((1-\omega)P_{c,\mathrm{f}}^{i,j}+\omega P_{c,\mathrm{f}}^{i,j+1}) = q_{t,\mathrm{f}}^{i,j+1}+Q_{t,\mathrm{f}}^{i,j+1}. \tag{59}$$

It is obtained by using the CCFD scheme to (59) that

$$\sum_{\gamma\in\partial e}\boldsymbol{\xi}_{a,\mathrm{f},\gamma}^{i,j+1}+\sum_{\gamma\in\partial e}((1-\omega)\boldsymbol{\xi}_{c,\mathrm{f},\gamma}^{i,j}+\omega\boldsymbol{\xi}_{c,\mathrm{f},\gamma}^{i,j+1}) = q_{t,\mathrm{f},e}^{i,j+1}|e|+Q_{t,\mathrm{f},e}^{i,j+1}|e|, \tag{60}$$

The matrix-fracture transfer is given by,

$$Q_{t,\mathrm{f},b}^{i,j+1} = -(Q_{t,\mathrm{f},b,K}^{i,j+1}+Q_{t,\mathrm{f},b,K'}^{i,j+1})/\epsilon, \tag{61}$$

$$Q_{t,\mathrm{f},b,K}^{i,j+1} = \boldsymbol{\xi}_{a,\mathrm{m},e,K}^{i,j+1}+(1-\omega)\boldsymbol{\xi}_{c,\mathrm{m},b,K}^{i,j}+\omega\boldsymbol{\xi}_{c,\mathrm{m},b,K}^{i,j+1}, \tag{62}$$

$$Q_{t,\mathrm{f},e,K'}^{i,j+1} = \boldsymbol{\xi}_{a,\mathrm{m},b,K'}^{i,j+1}+(1-\omega)\boldsymbol{\xi}_{c,\mathrm{m},b,K'}^{i,j}+\omega\boldsymbol{\xi}_{c,\mathrm{m},b,K'}^{i,j+1}, \tag{63}$$

where

$$\boldsymbol{\xi}_{a,\mathrm{m},b,K}^{i,j+1}\equiv\boldsymbol{\xi}_{a,\mathrm{m},b}^{i,j+1} = -|e|\chi_{t,\mathrm{mf},b}^{i,j}\frac{P_{w,\mathrm{f},b}^{i,j+1}-P_{w,\mathrm{m},K}^{i+1}}{d_{K,b}+\frac{\epsilon}{2}}, \tag{64}$$

$$\boldsymbol{\xi}_{c,\mathrm{m},b,K}^{i,j}\equiv\boldsymbol{\xi}_{c,\mathrm{m},b}^{i,j} = -|b|\chi_{c,\mathrm{mf},b}^{i,j}\frac{P_{c,\mathrm{f},b}^{i,j}-P_{c,\mathrm{m},K}^{i,j}}{d_{K,b}+\frac{\epsilon}{2}}, \tag{65}$$

$$\boldsymbol{\xi}_{c,\mathrm{m},b,K}^{i,j+1}\equiv\boldsymbol{\xi}_{c,\mathrm{m},b}^{i,j+1} = -|b|\chi_{c,\mathrm{mf},b}^{i,j}\frac{P_{c,\mathrm{f},b}^{i,j+1}-P_{c,\mathrm{m},K}^{i,j+1}}{d_{K,b}+\frac{\epsilon}{2}}, \tag{66}$$

along with

$$\chi^{i,j}_{t,\mathrm{mf},b} = \frac{(d_{K,b} + \frac{\epsilon}{2})\lambda^{i,j}_{t,\mathrm{f},K}\lambda^{i,j}_{t,\mathrm{m},K}\mathbf{K}_{\mathrm{f},K}\mathbf{K}_{\mathrm{m},K}}{\frac{\epsilon}{2}\lambda^{i,j}_{t,\mathrm{m},K}\mathbf{K}_{\mathrm{m},K} + d_{K,b}\lambda^{i,j}_{t,\mathrm{f},K}\mathbf{K}_{\mathrm{f},K}}, \tag{67}$$

$$\chi^{i,j}_{c,\mathrm{mf},b} = \frac{(d_{K,b} + \frac{\epsilon}{2})\lambda^{i,j}_{n,\mathrm{f},K}\lambda^{i,j}_{n,\mathrm{m},K}\mathbf{K}_{\mathrm{f},K}\mathbf{K}_{\mathrm{m},K}}{\frac{\epsilon}{2}\lambda^{i,j}_{n,\mathrm{m},K}\mathbf{K}_{\mathrm{m},K} + d_{K,b}\lambda^{i,j}_{n,\mathrm{f},K}\mathbf{K}_{\mathrm{f},K}}. \tag{68}$$

The treatment of the interface connecting multiple fractures is similar to (49). Therefore, in the time step used for the pressure in the fractures, we solve the following pressure equation

$$\mathbf{A}^{i,j}_{t,\mathrm{f}} P^{i,j+1}_{w,\mathrm{f}} = \mathbf{Q}^{i,j}_{t,\mathrm{f}}, \tag{69}$$

where

$$\mathbf{A}^{i,j}_{t,\mathrm{f}} = \mathbf{A}^{i,j}_{a,\mathrm{f},\mathrm{f}} - \omega\Delta t^{i,j}\Big(\mathbf{A}^{i,j}_{c,\mathrm{f},\mathrm{f}}P'_c(\mathbf{S}^{i,j}_{w,\mathrm{f}})\mathbf{M}^{-1}_{\mathrm{f}}\mathbf{A}^{i,j}_{w,\mathrm{f},\mathrm{f}} + \mathbf{A}^{i,j}_{c,\mathrm{f},\mathrm{m}}P'_c(\mathbf{S}^{i,j}_{w,\mathrm{m}})\mathbf{M}^{-1}_{\mathrm{m}}\mathbf{A}^{i,j}_{w,\mathrm{m},\mathrm{f}}\Big), \tag{70}$$

and

$$\begin{aligned}
\mathbf{Q}^{i,j}_{t,\mathrm{f}} \;=\; & \mathbf{Q}^{i,j+1}_{ac,\mathrm{f}} - \mathbf{A}^{i,j}_{a,\mathrm{f},\mathrm{m}}P^{i+1}_{w,\mathrm{m}} \\
& + \omega\Delta t^{i,j}\Big(\mathbf{A}^{i,j}_{c,\mathrm{f},\mathrm{m}}P'_c(\mathbf{S}^{i,j}_{w,\mathrm{m}})\mathbf{M}^{-1}_{\mathrm{m}}\mathbf{A}^{i,j}_{w,\mathrm{m},\mathrm{m}} + \mathbf{A}^{i,j}_{c,\mathrm{f},\mathrm{f}}P'_c(\mathbf{S}^{i,j}_{w,\mathrm{f}})\mathbf{M}^{-1}_{\mathrm{f}}\mathbf{A}^{i,j}_{w,\mathrm{f},\mathrm{m}}\Big)P^{i+1}_{w,\mathrm{m}} \\
& - \mathbf{A}^{i,j}_{c,\mathrm{f},\mathrm{m}}P_c(\mathbf{S}^{i,j}_{w,\mathrm{m}}) - \mathbf{A}^{i,j}_{c,\mathrm{f},\mathrm{f}}P_c(\mathbf{S}^{i,j}_{w,\mathrm{f}}) \\
& - \omega\Delta t^{i,j}\Big(\mathbf{A}^{i,j}_{c,\mathrm{f},\mathrm{m}}P'_c(\mathbf{S}^{i,j}_{w,\mathrm{m}})\mathbf{M}^{-1}_{\mathrm{m}}\mathbf{Q}^{i+1}_{w,\mathrm{m}} + \mathbf{A}^{i,j}_{c,\mathrm{f},\mathrm{f}}P'_c(\mathbf{S}^{i,j}_{w,\mathrm{f}})\mathbf{M}^{-1}_{\mathrm{f}}\mathbf{Q}^{i+1}_{w,\mathrm{f}}\Big).
\end{aligned} \tag{71}$$

In the above equations, the inverse of $\mathbf{M}_{\mathrm{m}}$ and $\mathbf{M}_{\mathrm{f}}$ is not expensive as they are diagonal. In the time step (t^i, t^{i+1}), we solve the linear system

(56) implicitly to obtain the pressure $P^{i+1}_{w,\mathrm{m}}$, and then in the time substep $(t^{i,j}, t^{i,j+1})$ compute $P^{i,j+1}_{w,\mathrm{f}}$ by solving (69).

Once the pressures $P^{i+1}_{w,\mathrm{m}}$ and $P^{i,j+1}_{w,\mathrm{f}}$ is obtained, the fluxes can be evaluated as described below. For a boundary b of matrix gridcell K, $\mathbf{n}_b$ is the unit normal vector pointing towards outside K. If $e \in \partial K \cap \partial K'$ and $b \nsubseteq \Omega_{\mathrm{f}}$,

$$\boldsymbol{\xi}^{i,j+1}_{a,\mathrm{m},b} = -|b|\chi^{i,j}_{t,b}\frac{P^{i+1}_{w,\mathrm{m},K'} - P^{i+1}_{w,\mathrm{m},K}}{d_{K,K'}}, \tag{72}$$

where

$$\chi^{i,j}_{t,b} = \frac{d_{K,K'}\lambda^{i,j}_{t,\mathrm{m},K}\lambda^{i,j}_{t,\mathrm{m},K'}\mathbf{K}_{\mathrm{m},K}\mathbf{K}_{\mathrm{m},K'}}{d_{K,b}\lambda^{i,j}_{t,\mathrm{m},K'}\mathbf{K}_{\mathrm{m},K'} + d_{K',b}\lambda^{i,j}_{t,\mathrm{m},K}\mathbf{K}_{\mathrm{m},K}}. \tag{73}$$

If $b \in \Omega_{\mathrm{f}} \cap \partial K \cap \partial K'$ and b is a fracture gridcell.

3.2. Multi-scale Time-Stepping for the Saturation Equation

The forward Euler scheme is used for time discretization of the saturation equation. in each time step used for the pressure in the fracture [17, 46, 18]. Now, let us divide the time-step $(t^{i,j}, t^{i,j+1}]$ of the fractures pressure into $N_{s,\mathrm{m}}$ sub-steps such that $(t^{i,j}, t^{i,j+1}] = \bigcup_{k=0}^{N_{s,\mathrm{m}}-1}(t^{i,j,k}, t^{i,j,k+1}]$, $t^{i,j,0} = t^{i,j}$ and $t^{i,j,N_{s,\mathrm{m}}} = t^{i,j+1}$. This time discretization is employed for the saturation in the matrix domain. Moreover, we use a smaller time-step size for the fracture saturation. Thus, we partition the time-step, $(t^{i,j,k}, t^{i,j,k+1}]$ into $N_{s,\mathrm{f}}$ time sub-steps as $(t^{i,j,k}, t^{i,j,k+1}] = \bigcup_{l=0}^{N_{s,\mathrm{f}}-1}(t^{i,j,k,l}, t^{i,j,k,l+1}]$, where $t^{i,j,k,0} = t^{i,j,k}$ and $t^{i,j,k,N_{s,\mathrm{f}}} = t^{i,j,k+1}$. Both the saturation equation in the matrix domain and in

the fractures network are solved explicitly as follows,

$$\phi_{\mathrm{m}}\frac{S_{w,\mathrm{m}}^{i,j,k+1}-S_{w,\mathrm{m}}^{i,j,k}}{\Delta t^{i,j,k}}+\nabla\cdot(f_{w,\mathrm{m}}^{i,j,k}\mathbf{u}_{a,\mathrm{m}}^{i,j+1})=q_{w,\mathrm{m}}^{i,j,k}, \tag{74}$$

and

$$\phi_{\mathrm{f}}\frac{S_{w,\mathrm{f}}^{i,j,k,l+1}-S_{w,\mathrm{f}}^{i,j,k,l}}{\Delta t^{i,j,k,l}}+\nabla\cdot(f_{w,\mathrm{f}}^{i,j,k,l}\mathbf{u}_{a,\mathrm{f}}^{i,j+1})=q_{w,\mathrm{f}}^{i,j,k,l}+Q_{w,\mathrm{f}}^{i,j,k}. \tag{75}$$

where $\triangle t^{i,j,k}=t^{i,j,k+1}-t^{i,j,k}$ and $\triangle t^{i,j,k,l}=t^{i,j,k,l+1}-t^{i,j,k,l}$. We use the upwind CCFD method to discretize the saturation equation (74),

$$|K|\phi_{\mathrm{m},K}\frac{S_{w,\mathrm{m},K}^{i,j,k+1}-S_{w,\mathrm{m},K}^{i,j,k}}{\Delta t^{i,j,k}}+\sum_{b\in\partial K}f_{w,b}^{i,j,k}\boldsymbol{\xi}_{a,\mathrm{m},b}^{i,j+1}=q_{w,\mathrm{m},K}^{i,j,k}|K|. \tag{76}$$

Let b be the interface between the matrix gridcells K and K'; that is, $b=\partial K\cap\partial K'$. If $b\nsubseteq\Omega_{\mathrm{f}}$, the term $f_{w,b}$ in (76) is given by,

$$f_{w,b}^{i,j,k}=\begin{cases}f_{w,\mathrm{m},K}^{i,j,k}, & \boldsymbol{\xi}_{a,\mathrm{m},b}^{i,j+1}>0,\\ f_{w,\mathrm{m},K'}^{i,j,k}, & \boldsymbol{\xi}_{a,\mathrm{m},b}^{i,j+1}<0.\end{cases} \tag{77}$$

If $b\subseteq\Omega_{\mathrm{f}}$ is a gridcell of the fracture network, the term $f_{w,b}$ in (76) becomes,

$$f_{w,b}^{i,j,k}=\begin{cases}f_{w,\mathrm{m},K}^{i,j,k}, & \boldsymbol{\xi}_{a,\mathrm{m},b}^{i,j+1}>0,\\ \widehat{f}_{w,\mathrm{f},b}^{i,j,k}, & \boldsymbol{\xi}_{a,\mathrm{m},b}^{i,j+1}<0,\end{cases} \tag{78}$$

where

$$\widehat{f}^{i,j,k}_{w,\mathrm{f},b} = \frac{1}{N_{s,\mathrm{f}}} \sum_{l=0}^{N_{s,f}-1} \frac{f^{i,j,k,l+1}_{w,\mathrm{f},b} + f^{i,j,k,l}_{w,\mathrm{f},b}}{2}. \tag{79}$$

It is analogous to discretize the saturation equation in the fracture system as

$$|b|\phi_{\mathrm{f},b}\frac{S^{i,j,k,l+1}_{w,\mathrm{f},b} - S^{i,j,k,l}_{w,\mathrm{f},b}}{\Delta t^{i,j,k,l}} + \sum_{\gamma\in\partial b} f^{i,j,k,l}_{w,\gamma}\boldsymbol{\xi}^{i,j+1}_{a,\mathrm{f},\gamma} = q^{i,j,k,l}_{w,\mathrm{f},\gamma}|e| + Q^{i,j,k,l}_{w,\mathrm{f},b}|b|, \tag{80}$$

where b is a gridcell of the fracture network. Let $\gamma = \partial b \cap \partial b'$ where b and b' are the fracture gridcells, then we have

$$f^{i,j,k,l}_{w,\gamma} = \begin{cases} f^{i,j,k,l}_{w,\mathrm{f},b}, & \boldsymbol{\xi}^{i,j+1}_{a,\mathrm{f},\gamma} > 0, \\ f^{i,j,k,l}_{w,\mathrm{f},b'}, & \boldsymbol{\xi}^{i,j+1}_{a,\mathrm{f},\gamma} < 0. \end{cases} \tag{81}$$

The volumetric transfer across the matrix-fracture interface b is given by

$$Q^{i,j,k,l}_{w,\mathrm{f},b} = -(f^{i,j,k,l}_{w,b,K}\boldsymbol{\xi}^{i,j+1}_{a,\mathrm{m},b,K} + f^{i,j,k,l}_{w,b,K'}\boldsymbol{\xi}^{i,j+1}_{a,\mathrm{m},b,K'})/\epsilon, \tag{82}$$

where

$$f^{i,j,k,l}_{w,b,K} = \begin{cases} f^{i,j,k}_{w,\mathrm{m},K}, & \boldsymbol{\xi}^{i,j+1}_{a,\mathrm{m},b,K} > 0, \\ f^{i,j,k,l}_{w,\mathrm{f},b}, & \boldsymbol{\xi}^{i,j+1}_{a,\mathrm{m},b,K} < 0. \end{cases} \tag{83}$$

In the above equations, the fluxes are obtained after solving the pressure equation.

To explicitly update of the saturation in the fractures, we use the previ-

ous matrix saturation in the matrix-fracture interfaces, and then obtain the matrix-vector form of (80),

$$\frac{1}{\Delta t^{i,j,k,l}}\mathbf{M}_{\mathrm{f}}\Big(\mathbf{S}_{w,\mathrm{f}}^{i,j,k,l+1}-\mathbf{S}_{w,\mathrm{f}}^{i,j,k,l}\Big)+\mathbf{A}_{s,\mathrm{f},\mathrm{f}}^{i,j+1}\mathbf{f}_{w,\mathrm{f}}^{i,j,k,l}+\mathbf{A}_{s,\mathrm{f},\mathrm{m}}^{i,j+1}\mathbf{f}_{w,\mathrm{m}}^{i,j,k}=\mathbf{Q}_{s,\mathrm{f}}^{i,j,k,l}. \quad (84)$$

After $N_{s,\mathrm{f}}$ smaller time steps, we update the saturation in the matrix domain by employing the following matrix-vector form of (75) as,

$$\frac{1}{\Delta t^{i,j,k,l}}\begin{bmatrix}\mathbf{M}_{\mathrm{m}} & \\ & \mathbf{M}_{\mathrm{f}}\end{bmatrix}\begin{bmatrix}\mathbf{S}_{w,\mathrm{m}}^{i,j,k,l+1}-\mathbf{S}_{w,\mathrm{m}}^{i,j,k,l}\\ \mathbf{S}_{w,\mathrm{f}}^{i,j,k,l+1}-\mathbf{S}_{w,\mathrm{f}}^{i,j,k,l}\end{bmatrix}+\begin{bmatrix}\mathbf{A}_{s,\mathrm{m},\mathrm{m}}^{i,j+1} & \mathbf{A}_{s,\mathrm{m},\mathrm{f}}^{i,j+1}\\ \mathbf{A}_{s,\mathrm{f},\mathrm{m}}^{i,j+1} & \mathbf{A}_{s,\mathrm{f},\mathrm{f}}^{i,j+1}\end{bmatrix}\begin{bmatrix}\mathbf{f}_{w,\mathrm{m}}^{i,j,k,l}\\ \mathbf{f}_{w,\mathrm{f}}^{i,j,k,l}\end{bmatrix}$$
$$=\begin{bmatrix}\mathbf{Q}_{s,\mathrm{m}}^{i,j,k,l}\\ \mathbf{Q}_{s,\mathrm{f}}^{i,j,k,l}\end{bmatrix}. \quad (85)$$

$$\frac{1}{\Delta t^{i,j,k}}\mathbf{M}_{\mathrm{m}}\Big(\mathbf{S}_{w,\mathrm{m}}^{i,j,k+1}-\mathbf{S}_{w,\mathrm{m}}^{i,j,k}\Big)+\mathbf{A}_{s,\mathrm{m},\mathrm{m}}^{i,j+1}\mathbf{f}_{w,\mathrm{m}}^{i,j,k}+\mathbf{A}_{s,\mathrm{m},\mathrm{f}}^{i,j+1}\widehat{\mathbf{f}}_{w,\mathrm{f}}^{i,j,k}=\mathbf{Q}_{s,\mathrm{m}}^{i,j,k}. \quad (86)$$

In (85) and (86), $\mathbf{A}_{s,\mathrm{m},\mathrm{f}}^{i,j+1}$ and $\mathbf{A}_{s,\mathrm{f},\mathrm{m}}^{i,j+1}$ indicate the interconnections of the saturation in the matrix blocks and fracture system.

3.3. Multi-scale explicit time-stepping for the concentration equation

On the other hand, as the nanoparticles concentrations vary more rapidly than the pressures (we assume a similar level of saturation discretization). We also use a smaller time-step size for the concentrations in matrix domain and the smallest time-step size for the concentrations in fractures. The

backward Euler time discretization is used for the equations of concentration and the deposited nanoparticles concentration on the pore–walls and entrapped nanoparticles concentration in the pore–throats. Therefore, the system of governing equations, (3), (5), (6), (10) and (11), is solved based on the adapted multiscale time-splitting technique. Therefore, the nanoparticles concentration, deposited nanoparticles concentration on the pore–walls and entrapped nanoparticles concentration in the pore–throats in the matrix domain are computed implicitly as follow,

$$\begin{aligned}
&\phi_{\mathrm{m}}\left(C_{s1,\mathrm{m}}^{i,j,k}, C_{s2,\mathrm{m}}^{i,j,k}\right)\frac{S_{w,\mathrm{m}}^{i,j,k+1}C_{\mathrm{m}}^{i,j,k+1}-S_{w,\mathrm{m}}^{i,j,k}C_{\mathrm{m}}^{i,j,k}}{\Delta t^{i,j,k}}+\\
&\nabla\cdot\left\{\mathbf{u}_{w,\mathrm{m}}^{i+1}C_{\mathrm{m}}^{i,j,k+1}-\phi_{\mathrm{m}}\left(C_{s1,\mathrm{m}}^{i,j,k}, C_{s2,\mathrm{m}}^{i,j,k}\right)S_{w,\mathrm{m}}^{i,j,k+1}D\left(C_{s1,\mathrm{m}}^{i,j,k}, C_{s2,\mathrm{m}}^{i,j,k}\right)\nabla C_{\mathrm{m}}^{i,j,k+1}\right\}=\\
&R\left(\mathbf{u}_{w,\mathrm{m}}^{i+1}, C_{\mathrm{m}}^{i,j,k+1}, C_{s1,\mathrm{m}}^{i,j,k}\right)+Q_{c,\mathrm{m}}^{i,j,k+1},
\end{aligned}\tag{87}$$

$$\frac{C_{s1,\mathrm{m}}^{i,j,k+1}-C_{s1,\mathrm{m}}^{i,j,k}}{\Delta t^{i,j,k}}=\begin{cases}\gamma_d|\mathbf{u}_{w,\mathrm{m}}^{k+1}|C_{\mathrm{m}}^{i,j,k+1}, & \mathbf{u}_{w,\mathrm{m}}^{i+1}\le u_r\\ \gamma_d|\mathbf{u}_{w,\mathrm{m}}^{k+1}|C_{\mathrm{m}}^{i,j,k+1}-\gamma_e|\mathbf{u}_{w,\mathrm{m}}^{k+1}-u_r|C_{s1,\mathrm{m}}^{i,j,k+1}, & \mathbf{u}_{w,\mathrm{m}}^{i+1}>u_r\end{cases}\tag{88}$$

and,

$$\frac{C_{s2,\mathrm{m}}^{i,j,k+1}-c_{s2,\mathrm{m}}^{i,j,k}}{\Delta t^{i,,j,k}}=\gamma_{pt}|\mathbf{u}_{w,\mathrm{m}}^{k+1}|C_{\mathrm{m}}^{i,j,k+1}\tag{89}$$

In the same manner, we consider the variations of nanoparticles concentrations in the fractures are faster than those in the matrix domain. So,

the nanoparticles concentration, the deposited nanoparticles concentration on the pore–walls and entrapped nanoparticles concentration in the pore–throats in the fractures are expressed as follow,

$$\phi_{\mathrm{f}}\left(C_{s1,\mathrm{f}}^{i,j,k,l}, C_{s2,\mathrm{f}}^{i,j,k,l}\right)\frac{S_{w,\mathrm{f}}^{i,j,k,l+1}C_{\mathrm{f}}^{i,j,k,l+1}-S_{w,\mathrm{f}}^{i,j,k,l}C_{\mathrm{f}}^{i,j,k,l}}{\Delta t^{i,j,k,l}}+$$
$$\nabla\cdot\left\{\mathbf{u}_{w,\mathrm{f}}^{i+1}C_{\mathrm{f}}^{i,j,k,l+1}-\phi_{\mathrm{f}}\left(C_{s1,\mathrm{f}}^{i,j,k,l}, C_{s2,\mathrm{f}}^{i,j,k,l}\right)S_{w,\mathrm{f}}^{i,j,k,l+1}D\left(C_{s1,\mathrm{f}}^{i,j,k,l}, C_{s2,\mathrm{f}}^{i,j,k,l}\right)\nabla C_{\mathrm{f}}^{i,j,k,l+1}\right\}=$$
$$R\left(\mathbf{u}_{w,\mathrm{f}}^{i+1}, C_{\mathrm{f}}^{i,j,k,l+1}, C_{s1,\mathrm{f}}^{i,j,k,l}\right)+Q_{c,\mathrm{f}}^{i,j,k,l+1}+Q_{c,\mathrm{m,f}}^{i,j,k,l+1}, \tag{90}$$

$$\frac{C_{s1,\mathrm{f}}^{i,j,k,l+1}-C_{s1,\mathrm{f}}^{i,j,k,l}}{\Delta t^{i,j,k}}=\begin{cases}\gamma_d|\mathbf{u}_{w,\mathrm{f}}^{k+1}|C_{\mathrm{f}}^{i,j,k,l+1}, & \mathbf{u}_{w,\mathrm{f}}^{i+1}\le u_r\\ \gamma_d|\mathbf{u}_{w,\mathrm{f}}^{k+1}|C_{\mathrm{f}}^{i,j,k,l+1}-\gamma_e|\mathbf{u}_{w,\mathrm{f}}^{k+1}-u_r|C_{s1,\mathrm{f}}^{i,j,k,l+1}, & \mathbf{u}_{w,\mathrm{f}}^{i+1}>u_r\end{cases} \tag{91}$$

and,

$$\frac{C_{s2,\mathrm{f}}^{i,j,k,l+1}-c_{s2,\mathrm{f}}^{i,j,k}}{\Delta t^{i,,j,k,l}}=\gamma_{pt}|\mathbf{u}_{w,\mathrm{f}}^{k+1}|C_{\mathrm{f}}^{i,j,k,l+1} \tag{92}$$

We use the upwind CCFD method to discretize the concentration equation (87),

$$|K|\phi_{\mathrm{m},K}\frac{S_{w,\mathrm{m},K}^{i,j,k+1}C_{\mathrm{m},K}^{i,j,k+1}-S_{w,\mathrm{m},K}^{i,j,k}C_{\mathrm{m},K}^{i,j,k}}{\Delta t^{i,j,k}}+\sum_{b\in\partial K}\hat{C}_{m,K}^{i,j,k+1}\mathbf{F}_{a,\mathrm{m},b}^{i,j+1}+\sum_{b\in\partial K}\mathbf{F}_{D,\mathrm{m},b}^{i,j,k+1}=$$
$$R\left(\mathbf{u}_{w,\mathrm{m}}^{i+1}, C_{\mathrm{m}}^{i,j,k+1}, C_{s1,\mathrm{m}}^{i,j,k}\right)|K|+Q_{c,\mathrm{m},K}^{i,j,k+1}|K|. \tag{93}$$

$$\mathbf{F}_{w,\mathrm{m},b}^{i,j+1}=\mathbf{u}_{w,\mathrm{m},b}^{i,j+1}|b|$$

Let b be the interface between the matrix gridcells K and K'; that is, $b = \partial K \cap \partial K'$. If $b \nsubseteq \Omega_{\mathrm{f}}$, the term $\hat{C}^{i,j,k+1}_{m,K}$ in (93) is given by,

$$\hat{C}^{i,j,k+1}_{m,K} = \begin{cases} C^{i,j,k}_{\mathrm{m},K}, & \mathbf{F}^{\mathbf{i,j+1}}_{\mathbf{w},\mathrm{m},\mathbf{b}} > \mathbf{0}, \\ C^{i,j,k}_{\mathrm{m},K'}, & \mathbf{F}^{\mathbf{i,j+1}}_{\mathbf{w},\mathrm{m},\mathbf{b}} < \mathbf{0}. \end{cases} \tag{94}$$

Now for the diffusion term; if $b \in \partial K \cap \partial K'$ and $b \nsubseteq \Omega_{\mathrm{f}}$, the fluxes in (93) are given by,

$$\mathbf{F}^{i,j,k+1}_{D,\mathrm{m},b} = -|b|\chi^{i,j,k+1}_{t,b} \frac{C^{i,j,k+1}_{\mathrm{m},K'} - C^{i,j,k+1}_{\mathrm{m},K}}{d_{K,K'}}, \tag{95}$$

where $\chi^{i,j,k}_{t,b}$ is given by the harmonic mean as,

$$\chi^{i,j,k+1}_{t,b} = \frac{d_{K,K'} D^{i,j,k}_{\mathrm{m},K} D^{i,j,k}_{\mathrm{m},K'} \phi^{i,j,k}_{\mathrm{m},K} \phi^{i,j,k}_{\mathrm{m},K'} S^{i,j,k+1}_{w,\mathrm{m},K} S^{i,j,k+1}_{w,\mathrm{m},K'}}{d_{K,b} D^{i,j,k}_{\mathrm{m},K'} \phi^{i,j,k}_{\mathrm{m},K'} S^{i,j,k+1}_{w,\mathrm{m},K'} + d_{K',b} D^{i,j,k}_{\mathrm{m},K} \phi^{i,j,k}_{\mathrm{m},K} S^{i,j,k+1}_{w,\mathrm{m},K}}, \tag{96}$$

On the other hand, if $b \in \Omega_{\mathrm{f}} \cap \partial K \cap \partial K'$ and b is a gridcell of the fracture system, we have,

$$\mathbf{F}^{i,j,k,l+1}_{D,\mathrm{m},b} \equiv \mathbf{F}^{i,j,k+1}_{D,\mathrm{m},b,K} = -|b|\chi^{i,j,k}_{t,\mathrm{mf},b} \frac{C^{i,j,k+1}_{\mathrm{f},b} - C^{i,j,k+1}_{\mathrm{m},K}}{d_{K,b} + \frac{\epsilon}{2}}, \tag{97}$$

where $\chi^{i,j,k,l+1}_{t,\mathrm{mf},b}$ is defined as,

$$\chi^{i,j,k,l+1}_{t,\mathrm{mf},b} = \frac{(d_{K,b} + \frac{\epsilon}{2}) D^{i,j,k}_{\mathrm{m},K} D^{i,j,k}_{\mathrm{f},K} \phi^{i,j,k}_{\mathrm{m},K} \phi^{i,j,k}_{\mathrm{f},K} S^{i,j,k+1}_{w,\mathrm{m},K} S^{i,j,k,l+1}_{w,\mathrm{f},K}}{\frac{\epsilon}{2} D^{i,j,k}_{\mathrm{m},K} \phi^{i,j,k}_{\mathrm{m},K} S^{i,j,k+1}_{w,\mathrm{m},K} + d_{K,b} D^{i,j,k}_{\mathrm{f},K} \phi^{i,j,k}_{\mathrm{f},K} S^{i,j,k,l+1}_{w,\mathrm{f},K}}, \tag{98}$$

It can be noted that in the presence of counter-current flows resulted from capillarity between matrix-fracture, the capillary pressure has a clear

contribution in the transfer fluxes as shown in (37), (38), (42), (43), (48), (49), (62), (63), (65) and (66). On the hand, for the counter-current flows resulted from gravity between matrix-fracture, all the transfer fluxes that define in terms of the pressure P_α, and the capillary pressure P_c, will be changed to be functions of their corresponding potentials, Φ_α and Φ_c, instead of P_α and P_c such that,

$$\Phi_\alpha = P_\alpha + \rho_\alpha g\mathbf{z},$$

and

$$\Phi_c = P_c + (\rho_n - \rho_w)g\mathbf{z}.$$

Therefore,

$$\mathbf{u}_a = -\lambda_t \mathbf{K}\nabla\Phi_w,$$

and

$$\mathbf{u}_c = -\lambda_n \mathbf{K}\nabla\Phi_c$$

4. Time-Steps Adaptation

Alternative to the manual implementation of the multi-stepping process, we can provide adaptive multi-stepping by verifying the Courant-Friedrichs-Lewy (CFL) condition to guarantee its satisfactory (i.e. CFL<1). Now, let us define the following CFLs,

$$\mathrm{CFL}_{m,x} = \frac{\mathbf{u}_x \Delta t^{i,j,k}}{\Delta x}, \tag{99}$$

$$\mathrm{CFL}_{m,y} = \frac{\mathbf{u}_y \Delta t^{i,j,k}}{\Delta y}, \tag{100}$$

for saturation and concentration in matrix blocks, and,

$$\mathrm{CFL}_{f,x} = \frac{\mathbf{u}_x \Delta t^{i,j,k,l}}{\Delta x}, \tag{101}$$

and

$$\mathrm{CFL}_{f,y} = \frac{\mathbf{u}_y \Delta t^{i,j,k,l}}{\Delta y}, \tag{102}$$

for for saturation and concentration in fractures. In implementation, each step we check if $\mathrm{CFL}_{m,x} > 1$ or $\mathrm{CFL}_{m,y} > 1$, the time-step of saturation/concentration in matrix will be divided by 2 and the $\mathrm{CFL}_{m,x}$ and $\mathrm{CFL}_{m,y}$ will be recalculated. This procedure will be repeated until satisfying the condition $\mathrm{CFL}_{m,x} < 1$ and $\mathrm{CFL}_{m,y} < 1$, then the final adaptive time-step saturation/concentration in matrix will be obtained. Similarly, we check if the condition, $\mathrm{CFL}_{f,x} > 1$ or $\mathrm{CFL}_{f,y} > 1$ is satisfied, the time-step of saturation/concentration in fractures will be divided by 2, then, we recalculate both $\mathrm{CFL}_{f,x}$ and $\mathrm{CFL}_{f,y}$. We repeat this procedure to satisfy the condition $\mathrm{CFL}_{f,x} < 1$ and $\mathrm{CFL}_{f,y} < 1$, to get the final adaptive time-step saturation/concentration in fractures.

We consider the following test to show how this scheme works. We select two different values of the number of steps of the outer loop, i, to be: (i=50, Fig. 1; i=100, Fig. 2). In these two figures, the adaptive time-step sizes, Δt^k and Δt^l are plotted against the number of steps of the outer loop i and the

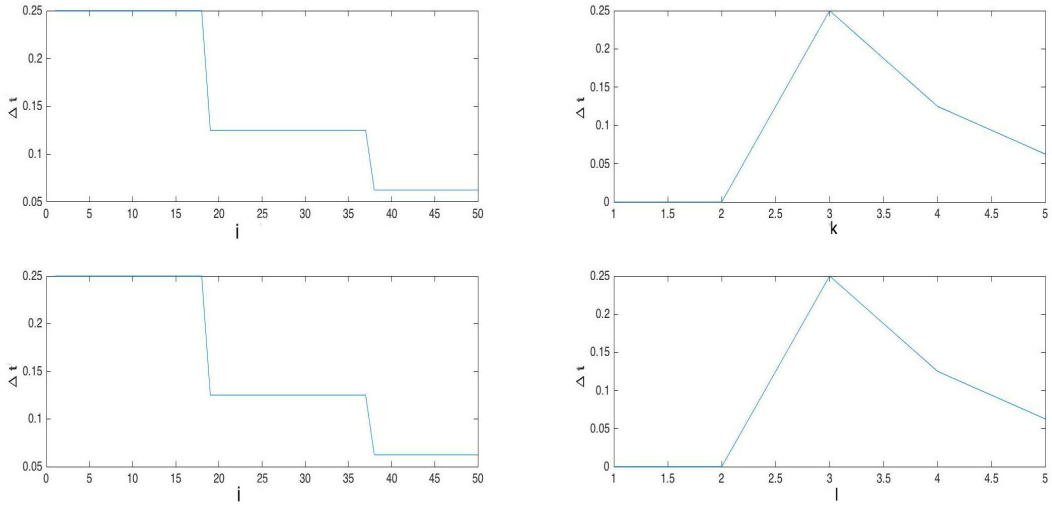

Figure 1: Adaptive time-step sizes, $\Delta t = \Delta t^k$ (upper) and $\Delta t = \Delta t^l$ (lower), against the number of steps of the outer loop i and the number of the inner loops k and l: Case 1 (Δt^i=50).

number of the inner loops k and l. It can be seen from these figures (Fig. 1 – Fig. 2) that the behavior of adaptive Δt^k and Δt^l are very similar. This may be because of the velocity is large and dominate the CFL. Also, both Δt^k and Δt^l start with large values then they gradually become smaller and smaller as i increases. On the other hand, for the two cases when i=50, 100, Δt^k and Δt^l are small when k and l are small, then they increase to reach a peak, and they are gradually decreasing.

5. Numerical Tests

In order to demonstrate the efficiency of the proposed scheme, we provide three numerical examples. Now, let us introduce some physical parameters

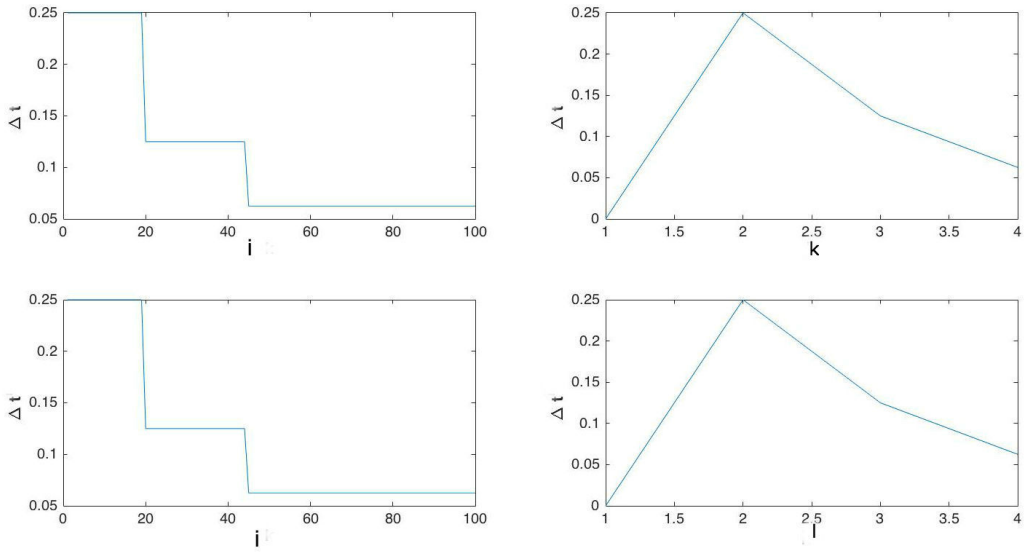

Figure 2: Adaptive time-step sizes, $\Delta t = \Delta t^k$ (upper) and $\Delta t = \Delta t^l$ (lower), against the number of steps of the outer loop i and the number of the inner loops k and l: Case 2 (Δt^i=100).

that used in the numerical tests. The normalized saturation S is defined as,

$$S_e = \frac{S_w - S_{rw}}{1 - S_{rw} - S_{rn}}, \tag{103}$$

where S_{rw} and S_{rn} are the residual saturations of the wetting and non-wetting phases, respectively. The capillary pressure function which is a function of the normalized saturation, [31, 47] is given by,

$$p_c(S_w) = -P_d \ln(S), \tag{104}$$

where P_d is the entry pressure. Also, the relative permeabilities of two phases are functions of the normalized saturation, are defined as,

$$k_{rw} = S^d, \tag{105}$$

$$k_{rn} = (1 - S)^d, \tag{106}$$

where d is a positive integer.

A domain of dimensions 10 m $\times$ 10 m $\times$ 1 m is employed for Examples 1 and 2, and each of them is composed of two fractures but they have different orientation (see Figs. 3 and 4. However, in Example 3, the domain has the dimensions, 20 m $\times$ 15 m $\times$ 1 m with multiple interconnected fractures as shown in Fig. 5. In Table 1, the physical and computational parameters are given.

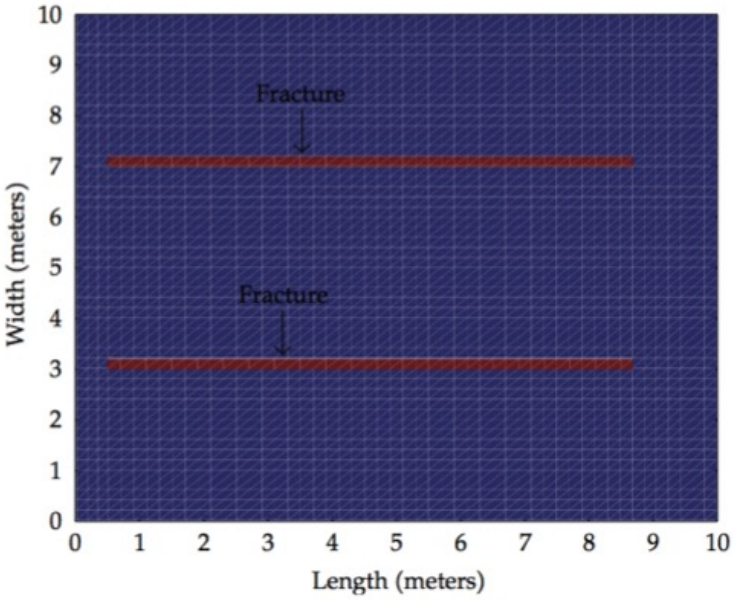

Figure 3: Distribution of fractures: Example 1.

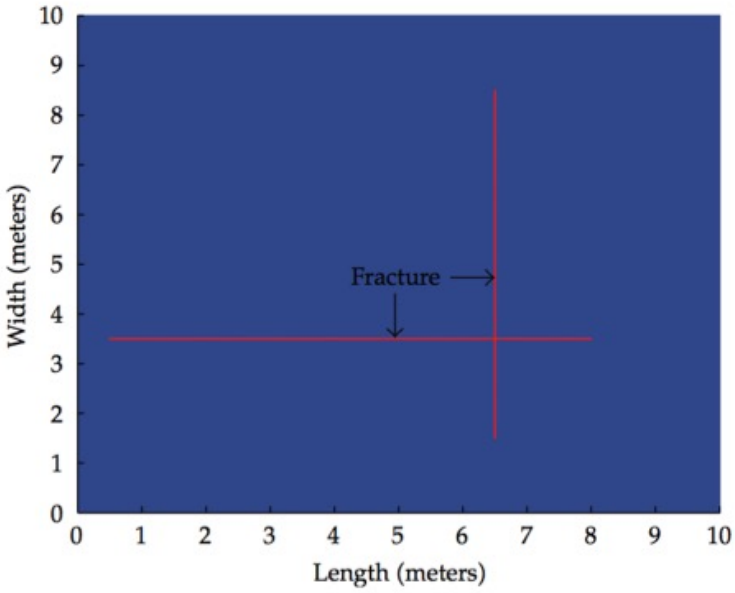

Figure 4: Distribution of fractures: Example 2.

Table 1: Physical and computational parameters of Examples 1-3.

Parameter	Example 1	Example 2	Examples 3
Domain dimensions (m)	$10 \times 10 \times 1$	$10 \times 10 \times 1$	$20 \times 15 \times 1$
Fracture aperture (m)	0.01	0.01	0.01
ϕ_{m}	0.2	0.2	0.15
ϕ_{f}	1	1	1
K_{m} (md)	1	1	50
K_{f} (md)	10^5	10^6	10^6
μ_w (cP)	1	1	1
μ_n (cP)	0.5	0.65	0.6
d	3	3	2
$P_{d,\mathrm{m}}$ (bar)	0.15	0.1	0.003
$P_{d,\mathrm{f}}$ (bar)	10^{-3}	10^{-4}	10^{-4}
S_{rw}	0	0	0
S_{rn}	0	0	0
Injection rate (PVI)	0.2	0.15	0.2
ω	1	1	0.5
Total gridcells	2704	2704	3300
Δt (days)	0.9827	1.6846	1.9010
$N_{p,\mathrm{f}}$	2	3	8
$N_{s,\mathrm{m}}$	6	5	5
$N_{s,\mathrm{f}}$	1	3	2
c_0	0.1	0.1	0.1

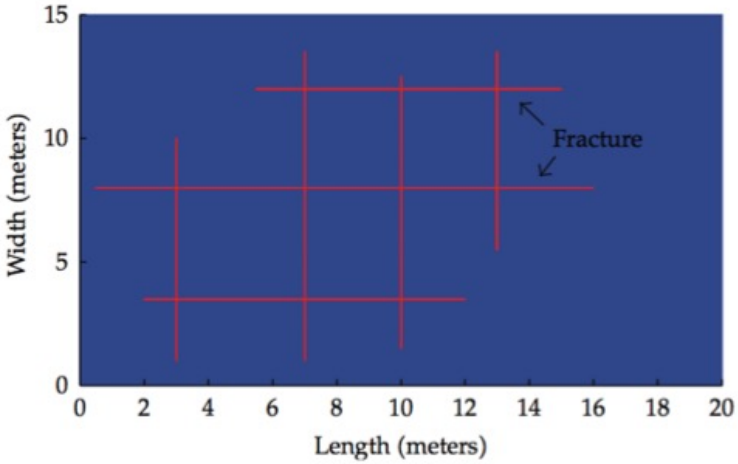

Figure 5: Distribution of fractures: Example 3.

The injection of the nanoparticles-water suspension into an oil reservoir is used to enhance oil recovery. In this example, we simulate the displacement process of oil by injecting the nanoparticles-water suspension with a rate of 0.2 pore volume injection (PVI) until 0.35 pore volume (PV). The nanoparticles concentration in the water is $c_0 = 0.1$ on the west boundary of the fractured domain. The permeability distribution of the fracture-matrix of example 1 is shown in Fig. 3. The physical and computational parameters are presented in Table 1. The permeability in the fractures is 10^5 md and in the matrix is 1 md, while, the viscosity of the oil is 0.5 cP. The total number of gridcells of matrix and fractures in example 1, is 2704. Also, Table 1 shows the outer (matrix pressure) time-step size $\Delta t = 0.9827$ and other levels of the multiple sub-timing numbers, namely, $N_{p,\mathrm{f}} = 2$, $N_{s,\mathrm{m}} = 6$ and $N_{s,\mathrm{f}} = 1$. These choices are sufficient for obtaining stable solutions by the proposed

multi-scale time strategy. Fig. 6 shows the water saturation distribution in the domain at 0.35 PV. From this figure, we may observe that the fluid moves rapidly inside the fractures and start to imbibe into the matrix at the end of the fracture faster than its beginning. The nanoparticles concentration distribution at 0.35 PV is presented in Fig. 7. As nanoparticles are carried by the water, the distribution of the nanoparticles concentration in the reservoir is very similar to the distribution of the water saturation. Moreover, the distribution of the concentration of deposited nanoparticles, c_{s1} is illustrated in Fig. 8. It can be seen from this figure that c_{s1} in the fracture is much higher than it in the matrix. Finally, the variations in both permeability and porosity of the fractured-medium due to nanoparticles adhering are presented in Figs. 9 and 10, respectively.

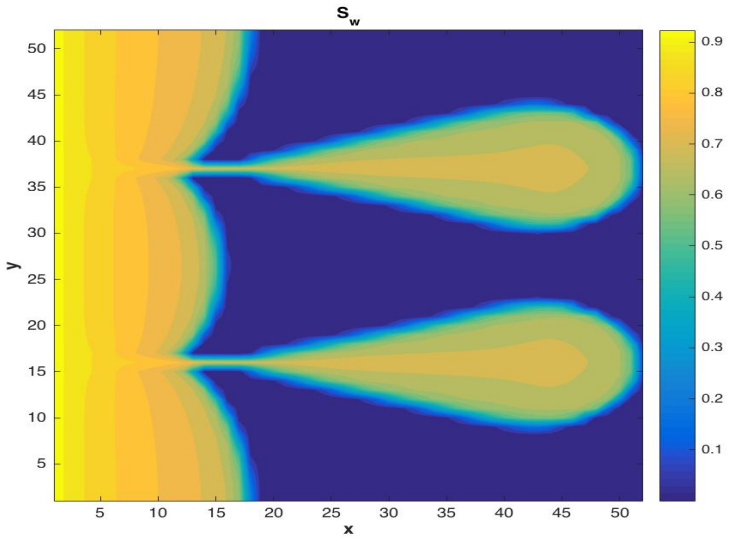

Figure 6: Distribution of the nanoparticles-water suspension saturation at 0.35 PV: Example 1.

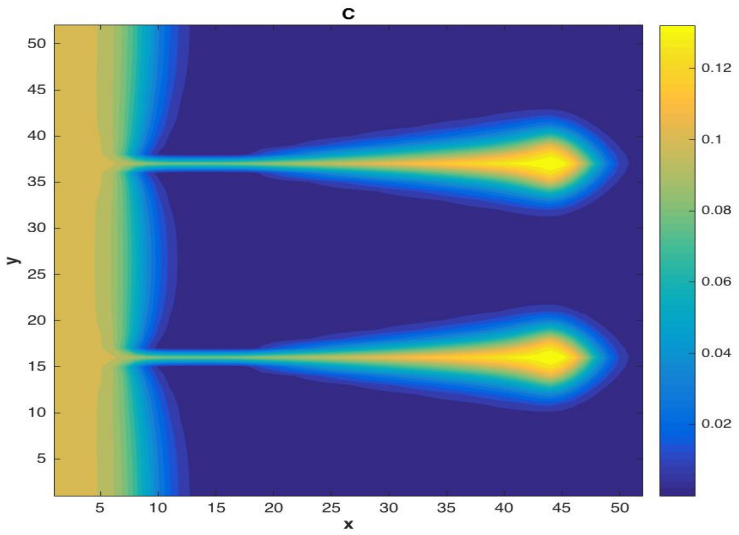

Figure 7: Distribution of the nanoparticles concentration at 0.35 PV: Example 1.

In Example 2, we have two interconnected fractures in the porous medium (see Fig. 4). The permeability in the matrix is 1 md and in fractures is 10^6 md, while, the viscosity of the oil is taken as 0.65 cP. The total number of matrices and fractures gridcells is 2704. In this example, the water injection rate is 0.15 PVI until 0.45 PV. The matrix-pressure time-step size is taken as $\Delta t = 1.6846$ and other levels of the multiple sub-timing numbers, namely, $N_{p,\mathrm{f}} = 3$, $N_{s,\mathrm{m}} = 5$ and $N_{s,\mathrm{f}} = 3$. More data and parameters can be found in Table 1. Also, we use the boundary nanoparticles concentration, $c_0 = 0.1$, on the west boundary of the fractured domain. The nanoparticles-water suspension saturation distribution in the fractured medium at 0.45 PV is shown in Fig. 11. This figure indicates that the nanoparticles-water suspension

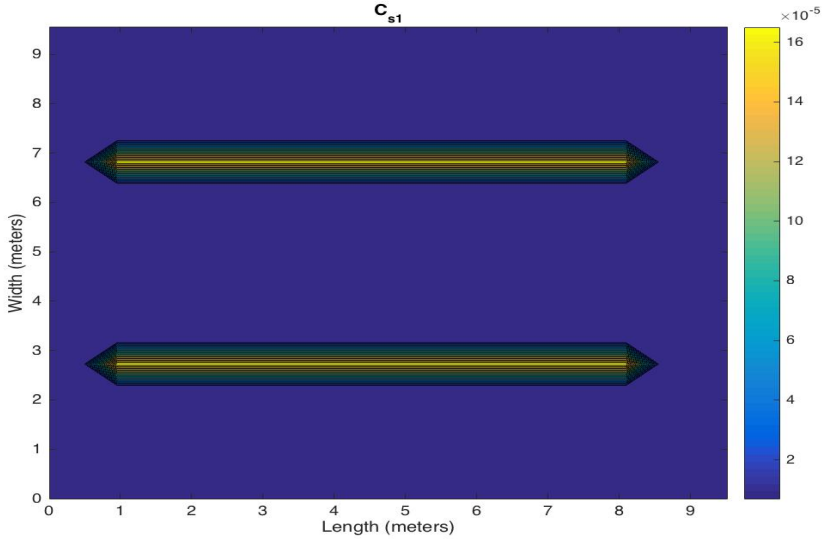

Figure 8: Distribution of the deposited nanoparticles concentration at 0.35 PV: Example 1.

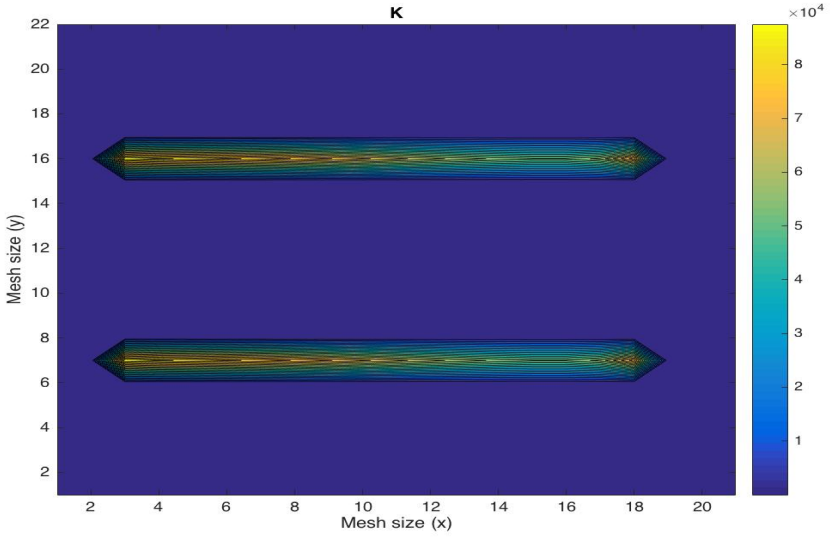

Figure 9: Distribution of the permeability variation at 0.35 PV: Example 1.

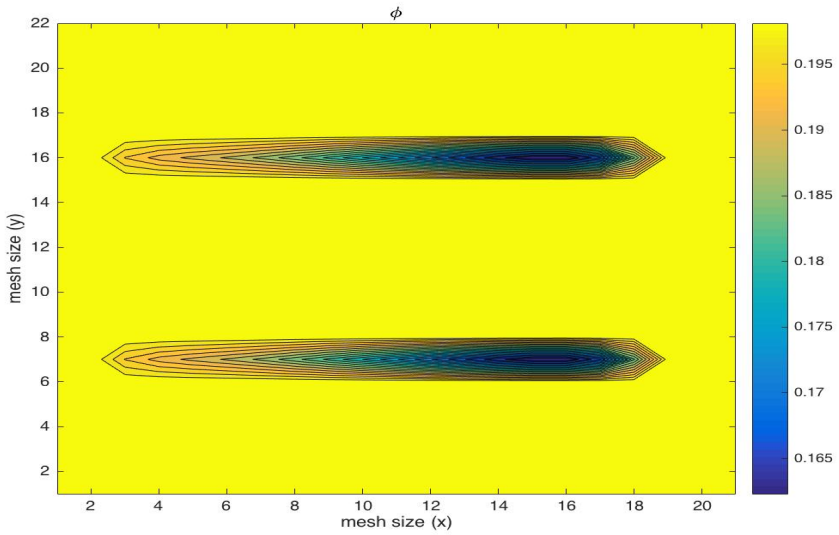

Figure 10: Distribution of the porosity of variation at 0.35 PV: Example 1.

transfers rapidly in the horizontal fracture into the other side of the fractured domain. So, fractures enhance the water distribution in the fractured medium. Also, the nanoparticles concentration profiles are shown in Fig. 12, while, Fig. 8 illustrates the distribution of the deposited nanoparticles concentration, c_{s1}. So, from these figures, we may again conclude that fractures exist in the medium enhance the distribution of the nanoparticles concentration. Moreover, the distribution of permeability and porosity variations are shown in Figs. 14 and 15, respectively. It is clear from these two figures that the permeability and the porosity variation are related to the deposited nanoparticles in the fractured medium.

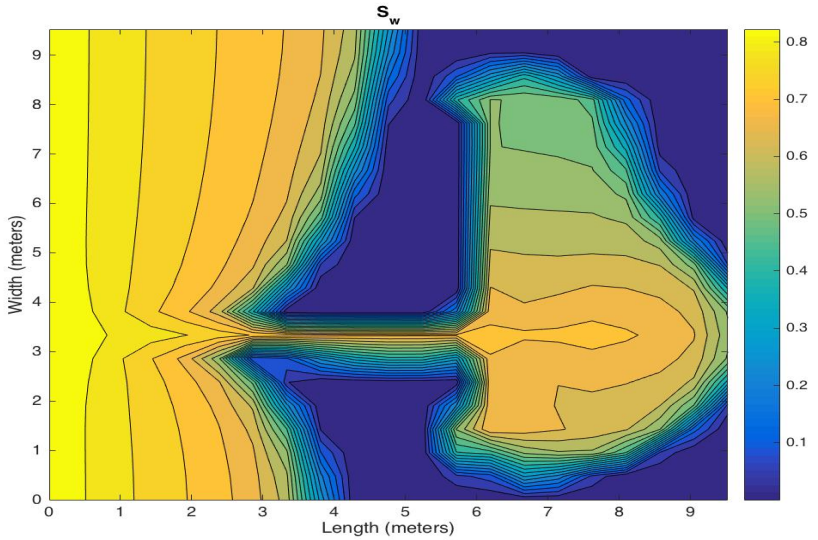

Figure 11: Distribution of the nanoparticles-water suspension saturation at 0.45 PV: Example 2.

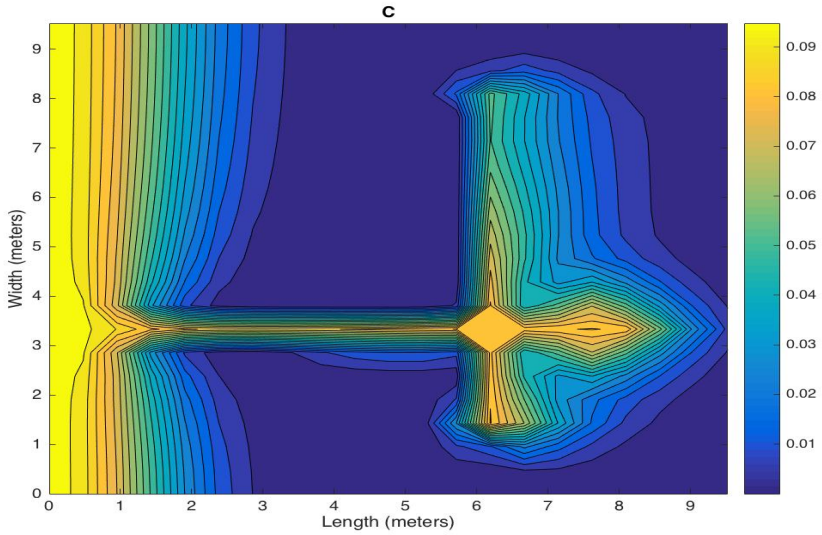

Figure 12: Distribution of the nanoparticles concentration at 0.45 PV: Example 2.

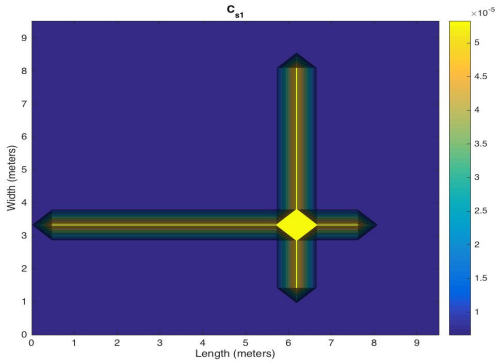

Figure 13: Distribution of the deposited nanoparticles concentration at 0.45 PV: Example 2

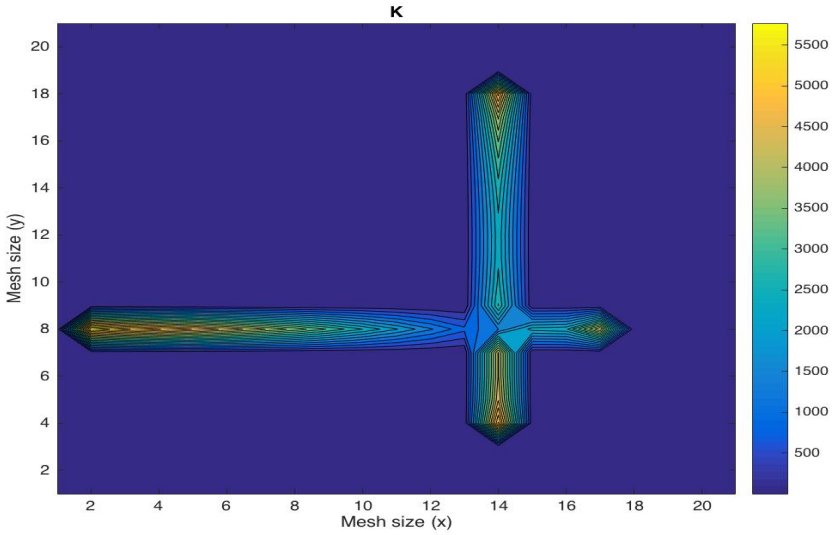

Figure 14: Distribution of the permeability variation at 0.45 PV: Example 2.

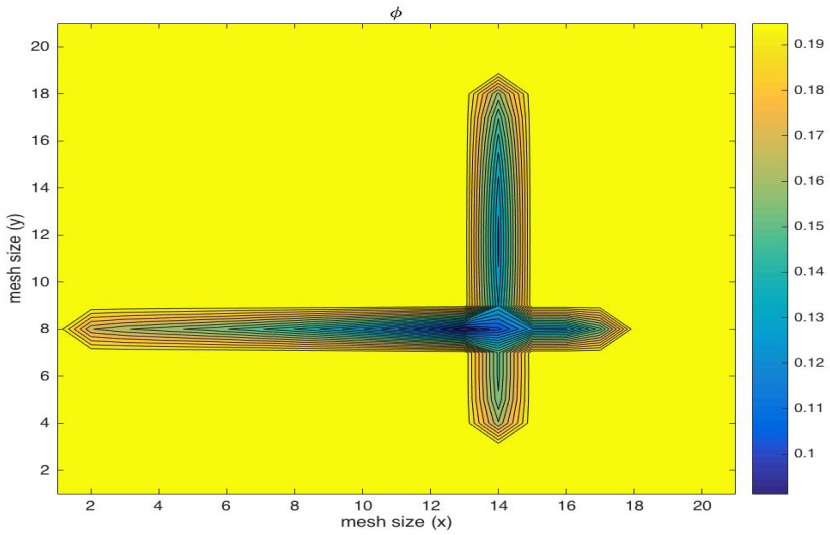

Figure 15: Distribution of the porosity variation at 0.45 PV: Example 2.

In Example 3, we consider a network composed of multiple interconnected fractures in the porous medium as shown in Fig. 5. The permeability in the matrix is 1 md, while, in fractures is 10^6 md. The oil viscosity is 0.6 cP. The total number of gridcells is 3300. The water injection rate is 0.2 PVI until 0.45 PV. The matrix-pressure time-step size is taken as $\Delta t = 1.9010$, $N_{p,\mathrm{f}} = 8$, $N_{s,\mathrm{m}} = 5$ and $N_{s,\mathrm{f}} = 2$. Other physical and computational data used in this example is provided in Table 1. For Example 3, the distribution of the nanoparticles-water suspension in the fractured medium at 0.5 PV is shown in Fig. 16. It can be noted from this figure that the nanoparticles-water suspension moves rapidly in the horizontal fractures. Fig. 17 shows the nanoparticles concentration in the fractured medium at 0.5 PV. Moreover, the distribution of the deposited nanoparticles concentration is presented in

Fig. 18.

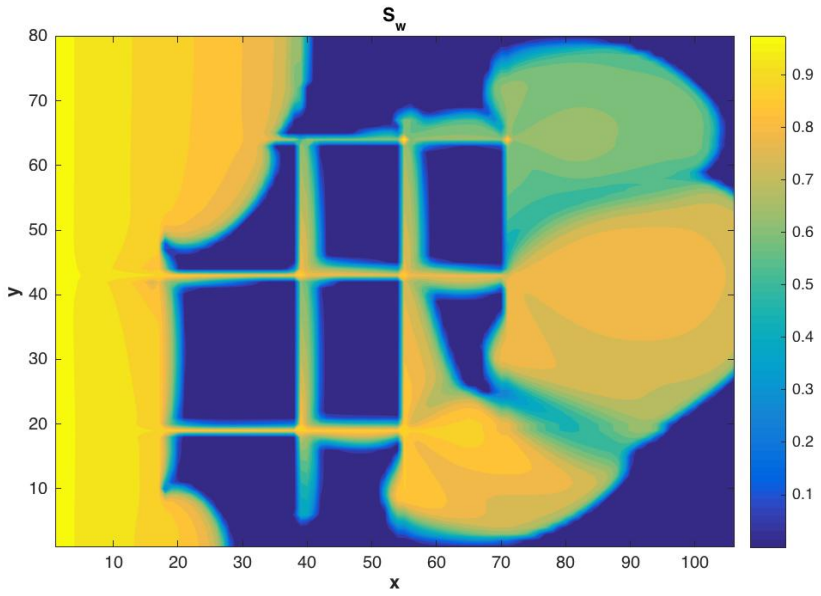

Figure 16: Distribution of the nanoparticles-water suspension saturation at 0.5 PV: Example 3.

6. Conclusions

In this paper, we studied the nanoparticles transport in two–phase flow in fractured porous media using multiscale time-stepping method. We used the IMPES-IMC scheme to solve the governing equations, and the CCFD method was used in the spatial discretization. A large time-step size is used in the matrix domain, while a smaller one is used in the fractures. The time-step of the pressure in fractures is partitioned into smaller subtime-steps, therefore, we

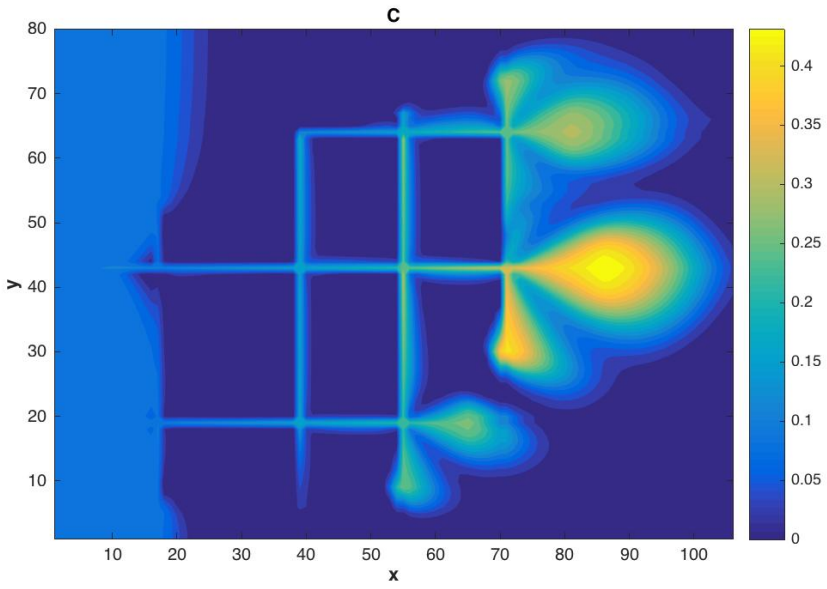

Figure 17: Distribution of the nanoparticles concentration at 0.5 PV: Example 3.

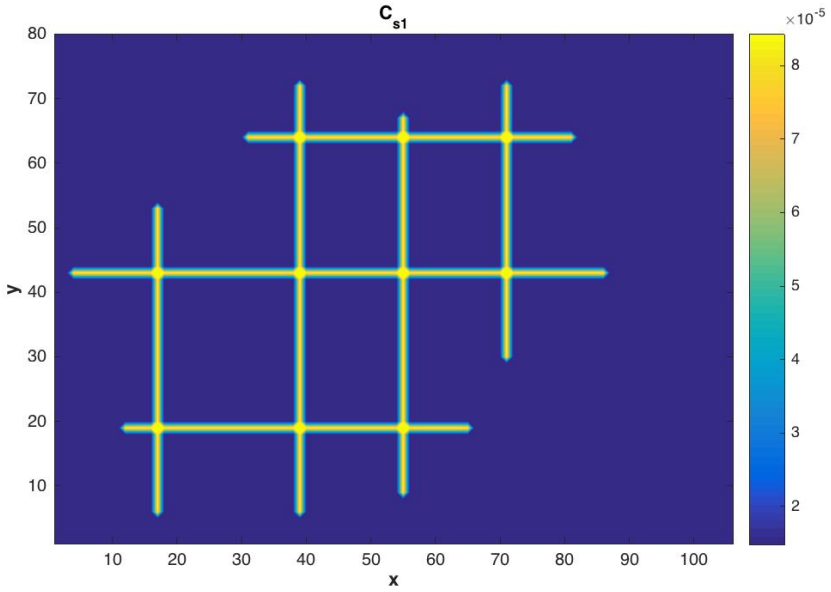

Figure 18: Distribution of the deposited nanoparticles concentration at 0.5 PV: Example 3.

update the saturation in the same level of time-discretization explicitly. Similarly, the saturation concentration, deposited concentration, and entrapped concentration have a bigger time-stepping in the matrix blocks, while finer ones in the fractures. In order to show the efficiency of the proposed scheme, three numerical examples with different configurations are provided. The nanoparticles-water suspension transfers rapidly through the fractures. So, existence of fractures in the oil-reservoir enhances the water distribution and therefore the oil recovery in the fractured medium.

7. References

[1] R. G. Baca, R. C. Arnett, and D. W. Langford, Modelling fluid flow in fractured-porous rock masses by finite-element techniques, International Journal for Numerical Methods in Fluids, vol. 4, no. 4, pp.337–348, 1984.

[2] G. Barenblatt, Y. Zheltov, and I. Kochina, Basic concepts in the theory of seepage of homogeneous fluids in fissurized rocks, Journal of Applied Mathematics and Mechanics, vol. 24, no. 5, pp. 1286–1303, 1983.

[3] Z. Chen, G. Huan, and Y. Ma, Computational Methods for Multiphase Flows in Porous Media, Computational Science and Engineering, SIAM, Philadelphia, Pa, USA, 2006.

[4] K. Ghorayeb and A. Firoozabadi, Numerical study of natural convection and diffusion in fractured porous media, SPE Journal, vol. 5, no. 1, pp. 12–20, 2000.

[5] H. Hoteit and A. Firoozabadi, An efficient numerical model for incompressible two-phase flow in fractured media, Advances in Water Resources, vol. 31, no. 6, pp. 891–905, 2008.

[6] H. Kazemi, Pressure transient analysis of naturally fractured reservoirs with uniform fracture distribution, Society of Petroleum Engineers Journal, vol. 9, no. 4, pp. 451–462, 1969.

[7] H. Kazemi, J. R. Gilman, and A. M. Elsharkawy, Analytical and numerical solution of oil recovery from fractured reservoirs with empirical transfer functions, SPE Reservoir Engineering , vol. 7, no. 2, pp. 219–227, 1992.

[8] H. Kazemi and L. S. Merrill, Numerical simulation of water imbibition in fractured cores, Old SPE Journal, vol. 19, no. 3, pp. 175–182, 1979.

[9] S. H. Lee, C. L. Jensen, and M. F. Lough, Efficient finite-difference model for flow in a reservoir with multiple length-scale fractures, SPE Journal, vol. 5, no. 3, pp. 268–275, 2000.

[10] J. Noorishad and M. Mehran, An upstream finite element method for solution of transient transport equation in fractured porous media, Water Resources Research, vol. 18, no. 3, pp. 588–596, 1982.

[11] K. Pruess and T. N. Narasimhan, A practical method for modeling fluid and heat flow in fractured porous media, Society of Petroleum Engineers journal, vol. 25, no. 1, pp. 14–26, 1985.

[12] S. Sarkar, M. N. Toksoz, and D. R. Burns, Fluid flow simulation in fractured reservoirs, in Report of the Annual Consortium Meeting, 2002.

[13] L. K. Thomas, T. N. Dixon, and R. G. Pierson, Fractured reservoir simulation, SPE Journal, vol. 23, no. 1, pp. 42–54, 1983.

[14] J. E. Warren and P.J. Root, "The behavior of naturally fractured reservoirs", Old SPE Journal, vol. 3, no. 3, pp. 245–255, 1963.

[15] K.H., Coats, IMPES stability: selection of stable time steps, SPE-84924, SPE ReservoirSimulation Symposium, Houston, TX, 2001.

[16] Z. Chen, G. Huan and Y. Ma, Computational methods for multiphase flows in porous media, SIAM Computational Science and Engineering, Philadelphia, 2006.

[17] L.C. Young and R.E. Stephenson, A generalized compositional approach for reservoir simulation", SPE Journal, vol. 23, pp. 727–742, 1983.

[18] J. Kou and S. Sun, A new treatment of capillarity to improve the stability of IMPES two-phase flow formulation, Computers and Fluids, vol. 39, pp. 1923–1931, 2010.

[19] J. Kou, S. Sun and B. Yu, Multiscale time-splitting strategy for multiscale multiphysics processes of two-phase flow in fractured media, Journal of Applied Mathematics, Article ID 861905, 2011.

[20] T. Belytschko and Y. Y. Lu, Convergence and stability analyses of multi-time step algorithm for parabolic systems, Computer Methods in Applied Mechanics and Engineering, vol. 102, no. 2, pp. 179–198, 1993.

[21] A. Gravouil and A. Combescure, Multi-time-step explicit–implicit method for non-linear structural dynamics, International Journal for Numerical Methods in Engineering, vol. 50, no. 1, pp. 199–225, 2000.

[22] M. Klisinski, Inconsistency errors of constant velocity multi-time step integration algorithms, Computer Assisted Mechanics and Engineering Sciences, vol. 8, no. 1, pp. 121–139, 2001.

[23] S. M. Bhallamudi, S. Panday, and P. S. Huyakorn, Sub-timing in fluid flow and transport simulations, Advances in Water Resources, vol. 26, no. 5, pp. 477–489, 2003.

[24] Y. J. Park, E. A. Sudicky, S. Panday, J. F. Sykes, and V. Guvanasen, Application of implicit sub-time stepping to simulate flow and transport in fractured porous media, Advances in Water Resources, vol. 31, no. 7, pp. 995–1003, 2008.

[25] V. Singh and S. M. Bhallamudi, Complete hydrodynamic border-strip irrigation model, Journal of Irrigation and Drainage Engineering, vol. 122, no. 4, pp. 189–197, 1996.

[26] V. Singh and S. M. Bhallamudi, Hydrodynamic modeling of basin irrigation, Journal of Irrigation and Drainage Engineering, vol. 123, no. 6, pp. 407–414, 1997.

[27] P. Smolinski, T. Belytschko, and M. Neal, Multi-time-step integration using nodal partitioning, International Journal for Numerical Methods in Engineering, vol. 26, no. 2, pp. 349–359, 1988.

[28] P. Smolinski, S. Sleith, and T. Belytschko, Stability of an explicit multi-time step integration algorithm for linear structural dynamics equations, Computational Mechanics. Solids, Fluids & Integrity, vol. 18, no. 3, pp. 236–243, 1996.

[29] S. Sun and J. Geiser, Multiscale discontinuous Galerkin and operator-splitting methods for modeling subsurface flow and transport, International Journal for Multiscale Computational Engineering, vol. 6, no. 1, pp. 87–101, 2008.

[30] J. E. VanderKwaak, Numerical simulation of flow and chemical transport in integrated surface-subsurface hydrologic systems, Ph.D. thesis, University of Waterloo, 1999.

[31] H. Hoteit and A. Firoozabadi, Numerical modeling of two-phase flow in heterogeneous permeable media with different capillarity pressures, Advances in Water Resources, vol. 31, pp. 56–73, 2008.

[32] C. Gruesbeck and R. E. Collins, Entrainment and deposition of fines particles in porous media, SPE Journal, vol. 24 , pp. 847–856, 1982.

[33] B. Ju and T. Fan, Experimental study and mathematical model of nanoparticle transport in porous media, Powder Technology, vol.192, pp. 195–202, 2009.

[34] X.H. Liu and F. Civian), Formation damage and skin factor due to filter cake formation and fines migration in the Near-Wellbore Region, SPE-27364, SPE Symposium on Formation Damage Control, Lafayette, Louisiana, 1994.

[35] M.F. El-Amin, A. Salama and S. Sun, Modeling and simulation of nanoparticles transport in a two-phase flow in porous media, SPE-154972, SPE International Oilfield Nanotechnology Conference and Exhibition, Noordwijk, The Netherlands, 2012.

[36] M.F. El-Amin, S. Sun and A. Salama, Modeling and simulation of nanoparticle transport in multiphase flows in porous media: CO_2 sequestration, SPE-163089, Mathematical Methods in Fluid Dynamics and Simulation of Giant Oil and Gas Reservoirs, 2012.

[37] M.F. El-Amin, S. Sun and A. Salama, Enhanced oil recovery by nanoparticles injection: modeling and simulation, SPE-164333, SPE Middle East Oil and Gas Show and Exhibition held in Manama, Bahrain, 2013.

[38] M.F. El-Amin, A. Salama and S. Sun, Numerical and dimensional analysis of nanoparticles transport with two–phase flow in porous media, Journal of Petroleum Science and Engineering, vol. 128, pp. 53–64, 2015.

[39] A. Salama, A. Negara, M.F. El-Amin, S. Sun, Numerical investigation of nanoparticles transport in anisotropic porous media, Journal of Contaminant Hydrology, vol. 181, pp. 114–130, 2015.

[40] H. Chen, Q. Di, F. Ye, C. Gu and J. Zhang, Numerical simulation of drag reduction effects by hydrophobic nanoparticles adsorption method in water flooding processes, Journal of Natural Gas Science and Engineering, vol. 35, pp. 1261–1269, 2016.

[41] M.H. Chen, A. Salama and M.F. El-Amin, Numerical aspects related to the dynamic update of anisotropic permeability field during the transport of nanoparticles in the subsurface, Procedia Computer Science, vol. 80, pp. 1382–1391, 2016.

[42] M.F. El-Amin, J. Kou, A. Salama and S. Sun, An iterative implicit scheme for nanoparticles transport with two-Phase flow in porous media, Procedia Computer Science, vol. 80, pp. 1344–1353, 2016.

[43] M.F. El-Amin, J. Kou and S. Sun, "Convergence analysis of the nonlinear iterative method for two-phase flow in porous media associated with nanoparticle injection, Int. J. Num. Meth. Heat Fluid Flow, To Appear, 2017.

[44] T. Arbogast, M.F. Wheeler and I. Yotov, Mixed finite elements for elliptic problems with tensor coefficients as cell-centered finite differences, SIAM Journal on Numerical Analysis, vol. 34, no. 2, pp. 828–852, 1997.

[45] J. Kou, S. Sun and B. Yu, Multiscale time-splitting strategy for multiscale multiphysics processes of two-phase flow in fractured media, Journal of Applied Mathematics, Article ID 861905, 2011.

[46] Z. Chen, G. Huan and B. Li, An improved IMPES method for two-phase flow in porous media, Transport in Porous Media, vol. 54, no. 3, pp. 361–376, 2004.

[47] M.F. El-Amin, A. Salama and S. Sun, Numerical and dimensional investigation of two-phase countercurrent imbibition in porous media, J. Computational Applied Mathematics, vol. 242, pp. 285–296, 2013.

[48] T. Crump, G. Ferte, A. Jivkov, P. Mummery and T. Van-Xuan, Dynamic fracture analysis by explicit solid dynamics and implicit crack propagation, Int. J. Solids and Structures, vol. 110?111, pp. 113-126, 2017.

[49] B. Lecampion and E. Detournay, An implicit algorithm for the propagation of a hydraulic fracture with a fluid lag, Computer Methods in Applied Mechanics and Engineering, vol. 196, pp. 4863-4880, 2007.